***Physics of Fluids (USA)***

***ACEEPTED May 1st 2024.***

# Transient dispersion of reactive solute transport in electrokinetic microchannel flow

Shan Huang,[1,] Sudip Debnath,[2,] Ashis Kumar Roy,[3, b)] Jiaming Wang,[1] Weiquan Jiang,[1, b)] **O. Anwar Bég[4] and S. Kuharat[4]**

[1)]*National Observation and Research Station of Coastal Ecological Environments in Macao; Macao Environmental Research Institute, Faculty of Innovation Engineering, Macau University of Science and Technology, 999078, Macao SAR, China.*

[2)]*Division of Mathematics, School of Advanced Sciences, Vellore Institute of Technology, Chennai-600127, India.*

[3)]*Department of Mathematics, Iswar Chandra Vidyasagar College, Belonia, Tripura -799155, India.*

[4)]*Multi-Physical Engineering Sciences Group, Mechanical Engineering Department, Corrosion Lab, 3-08, SEE Bldg, University of Salford, Manchester, England, UK.*

**Abstract**

Motivated by emerging applications in bio-microfluidic devices, the present study rigorously examines the generalized Taylor–Gill hydrodynamic dispersion of a point source solute injected into a microchannel, influenced by a constant axial static electric field along the channel and charged surface with different wall potentials. The solute engages in a first-order irreversible chemical reaction at both the microchannel walls. By incorporating different wall potentials and absorptive coefficients at the lower and upper walls, the current transport model for electro-osmotic flows is extended to encompass a wider range of applications. The solute transport phenomenon is intricately modelled using the unsteady convective diffusion equation. Employing Gill's generalized dispersion model, a concentration decomposition technique, up to the third-order accuracy, we meticulously analyse the transport process. Furthermore, a comprehensive comparison between analytical outcomes and numerical simulations using the Brownian Dynamics method is undertaken, enhancing the robustness of the analytical approach. The scattering process is mainly analyzed with the help of exchange, convection, dispersion and asymmetry coefficients, along with the mean concentration profile. The effect of initial solute release at various vertical locations in the microchannel is shown to exert a considerable impact on all the transport coefficients at initial times.

**Keywords:** *Microchannel flow, Reactive solute, Taylor-Gill dispersion, Electrokinetic, Brownian dynamics.*

***b) Authors to whom correspondence should be addressed: rk.ashis10@gmail.com and wqjiang@must.edu.mo***

## 1. INTRODUCTION

Hydrodynamic dispersion relates to the spreading of solute species molecules along the flow direction. It features in many diverse applications in medicine, engineering and environmental transport including hydrological river contamination[1], wetland contamination[2–5], chemical tracer transport in geochemistry[6], polymer pumping in shallow microchannels[7], rocket fuel injection systems[8], multicomponent distillation systems[9], dispersion of microorganisms[10,11], and cardiovascular hemodynamics[12]. Many further technological applications including chromatographic separation have been lucidly reviewed by Brenner and Edwards [13]. Taylor [14] pioneered the first comprehensive model of hydrodynamic dispersion in a seminal study on solute movement in a tube. He developed solutions considering pressure-driven transport through a conduit in the so-called long-time limit which is only valid for times much larger than the characteristic diffusion time for the species (time scale for equilibration in the direction perpendicular to the flow). Taylor [15] further refined his dispersion model. Via this model, it is known that dispersion enhances the rate of broadening of a solute cloud in flow through a conduit and furnishes a logical mechanism for accomplishing dilution or mixing. Taylor dispersion is similar to molecular diffusion, although it is actually produced via the complex interaction between transverse diffusion and velocity shear. Taylor dispersion is influenced by molecular (solute) diffusivity, viscosity, flow conditions and also conduit geometry, and is invariably associated with a non-uniform transverse velocity profile and a non-zero axial concentration gradient[16].

Many researchers subsequently investigated the Taylor dispersion phenomenon. Aris [17] considered axial and radial diffusion, generalizing the Taylor model. He later featured the convective-diffusion and phase exchange in molecular diffusion. Gill and Sankarasubramanian [18] addressed time-dependent behaviour and Gill and Sankarasubramanian [19] considered non-uniform mass transfer slug and transient diffusion effects. Additional subsequent investigations on Taylor dispersion were reported by Watson [20], and Hazra *et al.*[21] (for oscillatory current flows), Zeng *et al.* [22] and Wu *et al.* [23] (for tidal wetland flows). More recently investigators have also considered chemical reaction effects in Taylor dispersion. These can arise in biological fluid dynamics, microchannel systems and also chemical process engineering. Ng [24] developed asymptotic solutions for Taylor dispersion in advection–diffusion transport of a chemical species via a narrow conduit. He considered linear reversible (phase exchange or wall retention) and irreversible (decay or absorption) reactions at the conduit wall and also studied both cases of developed and transient concentrations. He showed that when phase exchange reaction kinetics is strong enough, the dispersion coefficient is strongly elevated via a modification in the conduit wall from non-retentive to mildly retentive. Ravikiran *et al.*[25] examined analytically the hydrodynamic dispersion of a solute in peristaltic flow of a biochemical incompressible micropolar biofluid in chyme digestive propulsion. They considered both combined homogeneous and

heterogeneous chemical reactions and using perturbation methods, showed that average effective dispersion coefficient is enhanced with peristaltic amplitude ratio Eringen vortex viscosity parameter and wall distensibility, while it is reduced with homogeneous and heterogeneous chemical reaction rates. Roy and Bég [26] investigated the Taylor dispersion in streaming blood flow in a rigid vessel with constant axial pressure gradient and first-order chemical reaction effects. They deployed a two-fluid model, simulating the core region as an Eringen micropolar fluid and the plasma surrounding layer as Newtonian viscous fluid. They presented exact solutions for the velocity and micro- rotation and deployed a Gill decomposition method to determine the solute (e.g. oxygen) concentration distribution. They showed that axial mean concentration peaks are depleted and migrate further along with the axial direction with larger values of Eringen vortex viscosity parameter and that transverse concentration is elevated with increasing micropolar coupling number and reaction rate. Further studies of Taylor dispersion with biochemical reactions include Roy *et al.* [27] (who included a Darcy-Forchheimer drag force model), Bég and Roy [28] (on statistical analysis of dual drug species dispersion) and Debnath *et al.*[29] (which included porous capillary walls).

The above studies have been confined to Newtonian or non-Newtonian transport and have neglected electromagnetic body force effects. In modern microfluidics, increasingly electrical (and magnetic fields) are being deployed to achieve enhanced control and manipulation capabilities in many areas of engineering. These include electro-osmotic micro/nanofluidics in actuator design[30], smart multifunctional nano-coatings[31], electrokinetic microfluidic pumps[32], droplet deposition[33], electro-chemical channels[34], electromagnetic sen- sors for nuclear reactors[35], microscale bio-robotics[36], ion drag pumps[37], dielectrics[38] and electromagnetic control of combustion processes[39]. Variously referred to as electro-kinetics or electrohydrodynamics (EHD), this discipline of modern fluid dynamics focuses on the interaction of electrical fields (either static or alternating) and viscous ionic liquids. It features in fertility control in biomechanics[40], capillary phase change devices in industrial heat transfer[41], bioinspired micro-pumping systems[42], electro-chemical surface modification in non-traditional machining[43] and next generation tunable coatings for naval and biomedical devices[44]. Electrical fields in all these applications have been shown to achieve exceptional effectiveness in controlling microscale (and nanoscale) phenomena which lead to improved de- signs. In particular, electro-kinetics in bio-microfluidics has grown in importance in the 21st century, due to many new exciting developments in bio-micro-electro-mechanical-systems (bioMEMS), bio-chip systems for drug delivery and biomedical diagnostics. Electro-kinetics involves the interaction of viscous flows (electrolytes) with an external electric field. It can feature many complex phenomena including Debye electric double layers (EDLs), zeta potential, spatial electrical conductivity gradient, electrical (Joule)

dissipation, ionic diffusion etc. A number of researchers have considered Taylor dispersion with electro-kinetic body force effects in recent years in the context of micro-fluidics[45,46].

In this area, the study of dispersion for relatively short times is of particular significance since transport processes occur rapidly in microfluidic devices and conduit lengths are generally small. Sadeghi *et al.* [47], presented closed-form solutions and finite-element nu- merical computations for steady electrokinetic Taylor solute dispersion in a polyelectrolyte layer-grafted rectangular microchannel with wall absorption effects. They considered a first- order irreversible reaction to simulate surface adsorption of solutes. They noted that the short-term transport coefficients are significantly modified by the initial concentration profile whereas the long-term values are not dependent upon the initial conditions. They further observed that the exchange and convection coefficients are elevated with an increment with the Damköhler number, whereas the dispersion coefficient is depleted. Additionally, they noted that with a larger EDL the extent of solute dispersion is widened. Hoshyargar *et al.* [48] computed the hydrodynamic dispersion in electro-osmotic flow through soft microchannels with small surface electrical potential. They derived closed-form solutions for the solute con- centration field and the effective dispersion coefficient. They noted that effective dispersion coefficient of a neutral solute band is considerably greater than for thicker polyelectrolyte layers (PEL), indicating that Taylor dispersion in electrokinetics is enhanced by attach- ing the PEL to the microchannel surface. Further studies of electro-Taylor dispersion in micro-conduits include the work by Roy *et al.*[46] (who considered Casson viscoplastic fluids), Murugan *et al.*[49] (who considered an axial electrical field and transverse magnetic field with boundary chemical reactions), Paul and Ng [50] (who included oscillatory electrical field and wall potential effects), Paul and Ng [51] (who included time-dependence) and Song *et al.*[52] (who addressed kinetic sorptive exchange at the microchannel boundaries).

A scrutiny of the scientific literature has revealed that thus far the electrokinetic Taylor hydrodynamic dispersion of a point source solute injected into a microchannel, influenced by a constant axial static electric field along the channel and charged surface with different wall potentials, has not been addressed. This is the focus of the current investigation. The solute is assumed to obey a first-order irreversible chemical reaction with both channel walls. Note that Sadeghi *et al.* [47] already considered the wall absorption in a three-dimensional mi- crochannel, while we only analyze the two-dimensional case. The crucial differences are: (i) this study considers absorption at both the microchannel walls and the reaction coefficients can be different from each other. Only a few previous studies[53–56] investigated this effect and they all focused on macroscopic flows such as wetland flows. (ii) the wall potentials at the microchannel walls can be different such that the electro-

osmotic flow can be asymmetric with respect to the centerline of the microchannel. These two distinctions can be considered as a generalization of the current transport model for electro-osmotic flows.

The aforementioned dispersion process will be modelled using the unsteady convective diffusion equation. Employing Gill's generalized dispersion model, a concentration decom- position technique, up to the third order accuracy, we carefully compute the transport processes. Furthermore, a comprehensive comparison between analytical solutions and numerical simulations using the Brownian Dynamics method is undertaken, enhancing the robustness of our analytical approach. The scattering process is mainly analysed with the help of exchange, convection, dispersion and asymmetry coefficients, along with the mean concentration profile. The effect of initial solute release at various heights of the channel has a considerable impact on all the transport coefficients. The study is relevant to bio-electro-microfluidic devices.

## 2.MATHEMATICAL ELECTROKINETIC DISPERSION MODEL

In the present work, we consider the transport of a neutral solute cloud (with concentration $C\ (x, y, t)$) in a laminar incompressible symmetric electrolyte solution through a parallel-plate narrow microchannel of height $H$, as shown in **Fig. 1**. A Cartesian coordinate system is used here to describe the problem mathematically, where the axial coordinate $x$ represents the axial flow direction, and the coordinate $y$ indicates the transverse direction of flow.

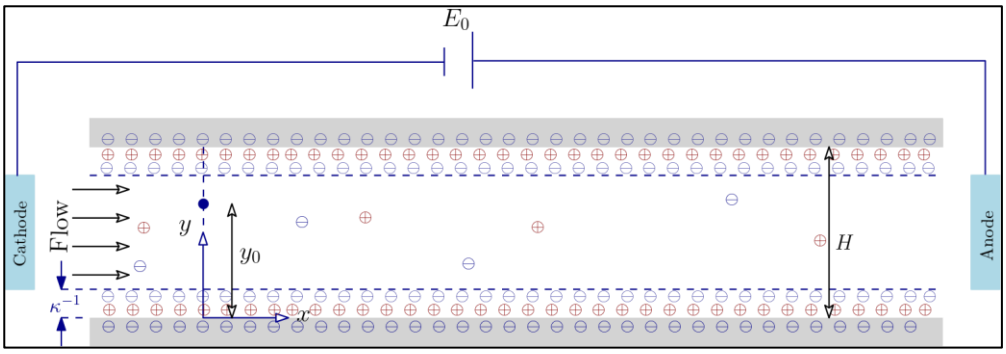


FIG. 1**.** Schematic diagram for electro-kinetic dispersion in a rectangular microchannel of height $H$. Electrokinetic flow inside the microchannel is generated by a static electric field $E_0$ in the *x-direction* and charged wall with different electric potential $\psi^1_{\text{wall}}$ (top wall) and $\psi^2_{\text{wall}}$ (bottom wall). A point source solute is released at height $y_0$ instantaneously which is dispersed in the microchannel and undergoes a linear first-order irreversible absorption with coefficients, $\beta_1$ and $\beta_0$, respectively.

The convection – diffusion equation for this regime is:

$$\frac{\partial C}{\partial t} + u\frac{\partial C}{\partial x} = D\left[\frac{\partial^2 C}{\partial x^2} + \frac{\partial^2 C}{\partial y^2}\right] \tag{1}$$

Here, $C$ is solute concentration, $t$ is time, $D$ is molecular diffusivity of the solute.

Also, the velocity field $u(y)$ is induced by a constant static external electric field $E_0$ applied in the axial direction.

This external electric field interacts with the EDL and creates the electrokinetic body force on the bulk fluid.

Let us consider a point source release in the micro-channel at a height $y_0$ from the centre of the channel with amount $n_r$, i.e.,

$$C(x, y, 0) = \frac{n_r}{H^3}\delta\left(\frac{x}{H}\right)\delta\left(\frac{y}{H} - \frac{y_0}{H}\right). \tag{2}$$

where $\delta(\cdot)$ is the Dirac delta function.

The injected solute is assumed to undergo a *linear first order irreversible absorption* according to the following relation:

$$\frac{\partial C}{\partial y} = \begin{cases} -\beta_1 C & \text{at} \quad y = H \\ \beta_0 C & \text{at} \quad y = 0 \end{cases} \tag{3}$$

Here $\beta_0$ and $\beta_1$ are the surface reaction rates at the lower and upper microchannel walls respectively. As a finite amount of solute is injected into the flow, it is reasonable to use the condition:

$$C(x = \pm\infty, y, t) = 0 \tag{4}$$

In order to study strategically the entire dispersion problem, in the forthcoming section, we will elaborately discuss one important component of the present problem, viz. velocity.

## Velocity solution

In the absence of a pressure gradient, the governing equation for the steady flow of ionized fluid, purely driven by a constant axial electric field $E_0$ is:

$$0 = \mu \frac{d^2u}{dy^2} + \rho_e E_0 \tag{5}$$

The classical no-slip boundary condition at the wall is prescribed:

$$u = 0 \text{ on } y = 0, H \tag{6}$$

Here μ the dynamic viscosity of fluid and is assumed to be independent of the local electric field strength, and $\rho_e$ the electric charge density.

The first term on the R.H.S. of (5) *viscous forcing term*, while the last term, i.e., $\rho_e E_0$, represents the *electrokinetic body force* (Coulomb force) under the shielding effect of the EDL formed next to the surface. This is the main driving force for generating the electro-osmotic flow (EOF), as noted by Saville [57] Electric charge density is given by the following relation:

$$\rho_e = -2ezc_0 \sinh\left(\frac{ze\psi}{k_B T}\right) \tag{7}$$

where $\psi$ is the electrokinetic potential, $c_0$ is the ion concentration far from the charged walls, $z$ is the valence of the co- and counter-ions in the carrier liquid, $e$ is the electron charge, $k_B$ is the Boltzmann constant, and $T$ is the absolute temperature. It is noteworthy that other charge density formulations are possible, and these will have a varied influence on the electro-kinetic transport. However, in the present study we have only considered the formulation based on eqn. (7). The charge potential $\psi$ can then be described by the following Poisson equation, giving the *net excess charge density* at a specific distance from the surface:

$$\frac{d^2\psi}{dy^2} = -\frac{\rho_e}{\varepsilon} \tag{8}$$

where $\varepsilon$ is the permittivity of the ionic fluid (electrolyte). Combination of Eqns. (7) and (8) gives rise to the famous *Poisson-Boltzmann equation*, which describes how the electrostatic potential varies in space due to the distribution of electrical charges:

$$\frac{\mathrm{d}^2\psi}{\mathrm{d}y^2} = \frac{2ezc_0}{\varepsilon}\sinh\left(\frac{ze\psi}{k_BT}\right) \tag{9}$$

If the electric potential is sufficiently small, typically when $\psi \le \psi_0 \approx 25\mathrm{mV}$, the Debye-Hückel approximation can be applied to Eq. (9). This results in the following *linear* equation:

$$\frac{\mathrm{d}^2\psi}{\mathrm{d}y^2} = \frac{2e^2z^2c_0}{\varepsilon k_BT}\psi = \frac{\psi}{\Lambda^2}, \tag{10}$$

Here $\Lambda = \left(\varepsilon k_BT / 2e^2z^2c_0\right)^{1/2}$ is the characteristic electrical double layer (EDL) thickness or the Debye length. Thus, we arrive at:

$$\frac{\mathrm{d}^2\psi}{\mathrm{d}y^2} = k^2\psi \tag{11}$$

Here $k = \Lambda^{-1}$ is the reciprocal of the Debye length, which is also known as the Debye – Hückel parameter. A larger value of $k$ thus corresponds to a thinner double layer, whereas for a thicker double layer $k$ is smaller. The boundary conditions for Eqn. (11) are given by:

$$\psi = \psi^1_{\mathrm{wall}} \quad \text{at } y = H \tag{12a}$$

$$\psi = \psi^2_{\mathrm{wall}} \quad \text{at } y = 0 \tag{12b}$$

The solution of Eqn. (11) subject to boundary condition (12) is

$$\psi(y) = \frac{\psi^1_{\mathrm{wall}}}{\sinh(kH)}\left[\psi^{12}_{\mathrm{wall}}\sinh\{k(H-y)\} + \sinh(ky)\right] \tag{13}$$

Here $\psi^{12}_{\mathrm{wall}}$ is the ratio of the two microchannel wall electrical potentials $\psi^{12}_{\mathrm{wall}} = \psi^2_{\mathrm{wall}} / \psi^1_{\mathrm{wall}}$. It is noteworthy that vector electric field is principally responsible for generating the driving force and will induce

skewness in the computed velocity distributions with amplification in the *y*- component of the electric field and the direction of skewness will be controlled by the polarity.

Substituting Eqs. (8) and (11) into Eq. (5), the governing equation becomes:

$$\frac{\mathrm{d}^2 u}{\mathrm{d}y^2} + k^2 U_{HS} \frac{\psi}{\psi^1_{\text{wall}}} = 0 \tag{14}$$

Here $U_{HS} = -\varepsilon E_0 \psi^1_{\text{wall}} / \mu$ is the so-called *Helmholtz Smoluchowski* velocity.

The solution of Eq. (14) with the aid of boundary condition (6) yields:

$$u(y) = U_{HS}\left[\psi^{12}_{\text{wall}}\left\{1 - \frac{y}{H} - \frac{\sinh(k\{H-y\})}{\sinh(kH)}\right\} - \frac{\sinh(ky)}{\sinh(kH)} + \frac{y}{H}\right] \tag{15}$$

## Dimensionless formulation

We introduce the following dimensionless parameters:

$$\begin{aligned} &\eta = \frac{y}{H}, \quad \eta_0 = \frac{y_0}{H}, \quad \xi = \frac{1}{Pe}\frac{x}{H} - \tau, \quad Pe = \frac{U_{HS} H}{D}, \quad \tau = \frac{Dt}{H^2}, \\ &\mathrm{U} = \frac{u - U_{HS}}{U_{HS}}, \quad \Omega = \frac{CH^3}{n_r}, \quad \Gamma_1 = \beta_1 H, \quad \Gamma_0 = \beta_0 H, \quad \kappa = kH. \end{aligned} \tag{16}$$

Here $\eta$ is dimensionless transverse coordinate, *$\eta o$ is transverse coordinate distance to the point source,$\xi$ is dimensionless axial coordinate, Pe is Péclet number (ratio of advection and effective diffusion), $\tau$ is dimensionless time, U is non-dimensional Helmholtz Smoluchowski velocity ratio, $\Omega$ is dimensionless point source solute mass, $\Gamma_0$, $\Gamma_1$ are the dimensionless surface reaction rates at the lower and upper microchannel walls, $\kappa$ is the EDL thickness (a smaller $\kappa$ implies larger Debye length).* The non-dimensional equation for the velocity distribution is:

$$\mathrm{U}(\eta) = (1 - \psi^{12}_{\text{wall}})(\eta - 1) - \frac{\psi^{12}_{\text{wall}} \sinh(\kappa\{1-\eta\}) + \sinh(\kappa\eta)}{\sinh(\kappa)} \tag{17}$$

Typically, the value of $\kappa$ is large, i.e., $O(10) - O(100)$ (see Paul and Ng [50,51], Song *et al.*[52] ).

Note that $\psi_{\text{wall}}^{12}$ represents the electrical potential of the base wall relative to that of the top wall, which is kept between -1 and 1(see Song *et al.*[52] ). It is clear from $\mathrm{U}(\eta)$ that fluid velocity is mostly controlled by the parameters $\kappa$ and $\psi_{\text{wall}}^{12}$. In Fig. 2, the velocity profiles are drawn for $\kappa$ when the ratio of wall potential is 0.5 and 1. It has been observed from Fig. 2 that the flow is asymmetric with respect to the centreline of the microchannel due to different wall potentials, whereas, symmetric when both the wall potentials are unique. Further, as $\kappa$ increases from Fig. 2(a) we can see maximum velocity appear near $\eta = 1$. Also, when $\psi_{\text{wall}}^{12} = 1$ the velocity profile remains parabolic for smaller $\kappa$ (Fig. 2(b)). If we increase the value of κ, it will result in a more friction factor as well as the apparent viscosity. Thus, the profile follows a plug flow like character.

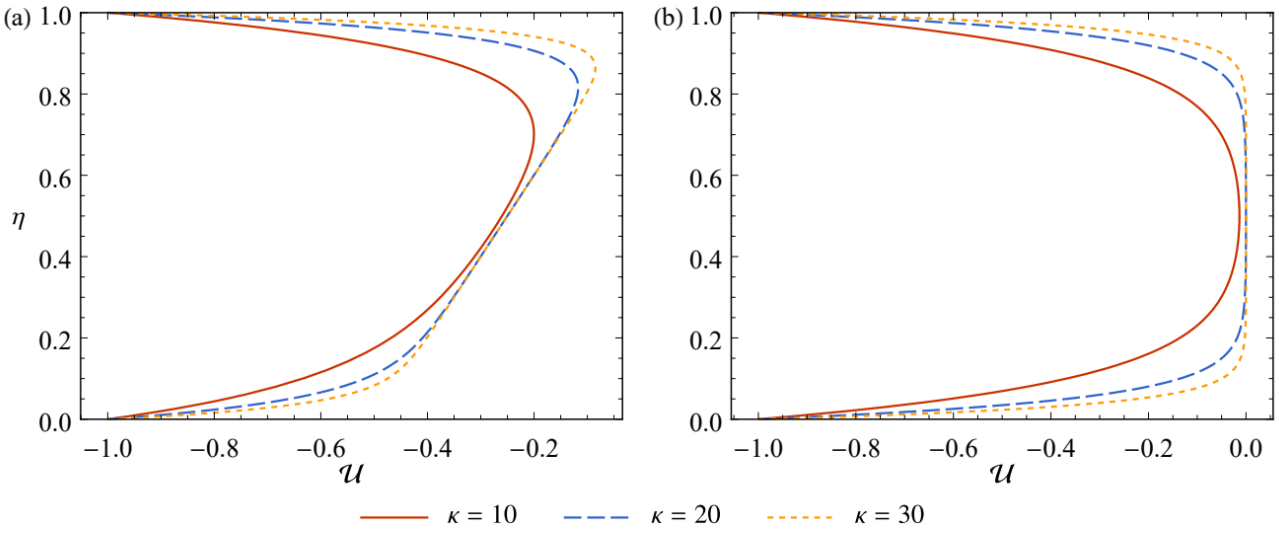


FIG. 2. Velocity profile $\mathrm{U}(\eta)$ of microchannel flows for different Debye--Hückel parameter values (κ): (a) an asymmetric electro-osmotic flow with respect to the centreline of the microchannel with different wall potentials ( $\psi_{\text{wall}}^{12} = 0.5$ ), and (b) a symmetric flow with the same wall potentials ( $\psi_{\text{wall}}^{12} = 1$ )

It follows that the governing equation and the initial and boundary conditions may be rewritten as follows:

$$\frac{\partial \Omega}{\partial \tau} + \mathrm{U}\frac{\partial \Omega}{\partial \xi} = \frac{1}{\mathrm{Pe}^2}\frac{\partial^2 \Omega}{\partial \xi^2} + \frac{\partial^2 \Omega}{\partial \eta^2}, \tag{18a}$$

$$\Omega(\xi, \eta, 0) = \delta(\xi)\delta(\eta - \eta_0) \tag{18b}$$

$$\frac{\partial \Omega}{\partial \eta} = \begin{cases} -\Gamma_1 \Omega & \text{at} \quad \eta = 1 \\ \Gamma_0 \Omega & \text{at} \quad \eta = 0 \end{cases} \tag{18c}$$

$$\Omega(\xi = \pm\infty, \eta, \tau) = 0 \tag{18d}$$

## 3.GENERALIZED DISPERSION MODEL

### Taylor–Gill hydrodynamic dispersion equation

We use the generalized dispersion model developed by Gill[58] to analyse the entire hydrodynamic problem defined by Eq. (18). The main focus of the generalized dispersion model is to expand the concentration distribution distribution in terms of the longitudinal derivatives of the cross-sectional mean concentration[59,60]. Adopting this procedure, for the current problem, we have:

$$\Omega = \sum_{n=0}^{\infty} f_n(\eta, \tau) \frac{\partial^n \bar{\Omega}}{\partial \xi^n}, \tag{19}$$

where $f_n$ are transverse coefficient functions to be determined later. $\langle \Omega \rangle$ is the mean con- centration distribution. We have used the brackets to denote the cross-sectional average operation, viz,

$$\langle f(\eta) \rangle \equiv \int_0^1 f(\eta)\, \mathrm{d}\eta, \tag{20}$$

The boundary condition of the coefficients $f_n$ is the same as (21) of $\Omega$:

$$\frac{\partial f_n}{\partial \eta} = \begin{cases} -\Gamma_1 f_n & \text{at} \quad \eta = 1, \\ \Gamma_0 f_n & \text{at} \quad \eta = 0, \end{cases} \tag{21}$$

where $f$ is an arbitrary function of the transverse coordinate $\eta$.

Now that taking the cross-sectional mean of (19) gives:

$$\langle f_0 \rangle = 1, \quad \langle f_n \rangle = 0, \quad n = 1, 2, 3, \ldots. \tag{22}$$

The boundary condition of the coefficients $f_n$ is the same as (18c) of $\Omega$:

$$\frac{\partial f_n}{\partial \eta} = \begin{cases} -\Gamma_1 f_n & \text{at } \eta = 1, \\ \Gamma_0 f_n & \text{at } \eta = 0, \end{cases} \tag{23}$$

for $n = 0,1,2,\ldots$. According to Eq. (18b), we can obtain the initial conditions of $f_n$:

$$f_0 \,|_{\tau=0} = \delta(\eta - \eta_0), \quad f_n \,|_{\tau=0} = 0, \quad n = 1,2,3,\ldots.$$

The next step of the generalized dispersion model is to obtain the essential Taylor--Gill expansion equation of $\langle \Omega \rangle$. Substituting Eq. (19) into Eq. (18a) and taking the cross-section average operation over $\eta$, we obtain the *Taylor - Gill dispersion model*:

$$\frac{\partial \langle \Omega \rangle}{\partial \tau} = \sum_{n=0}^{\infty} K_n(\tau) \frac{\partial^n \langle \Omega \rangle}{\partial \xi^n}, \tag{24}$$

Here the transport coefficients $K_n(\tau)$ are given by:

$$K_n(\tau) = \left\langle \frac{f_{n-2}}{Pe^2} \right\rangle + \left. \frac{\partial f_n}{\partial \eta} \right|_{\eta=0}^{\eta=1} - \langle \mathrm{U} f_{n-1} \rangle, \tag{25}$$

where $n = 0,1,2,\ldots$ and we take $f_{-1} = f_{-2} \equiv 0$ (auxiliary terms). Note that the exchange coefficient $K_0$ represents the solute depletion caused by wall absorption. $K_1$ and $K_2$ are coefficients related to the *advection and dispersion*, respectively. Finally, we determine the governing equation for $f_n(\eta, \tau)$. Substituting Eq. (19) into Eq. (18a) and comparing the coefficients of the longitudinal derivatives at each order, we have

$$\frac{\partial f_n}{\partial \tau} = \frac{\partial^2 f_n}{\partial \eta^2} - \mathrm{U} f_{n-1} + \frac{1}{Pe^2} f_{n-2} - \sum_{m=0}^{n} K_m f_{n-m}, \tag{26}$$

for $n = 0,1,2,\ldots$.

## Solutions of transport coefficients and the dispersion model

We have obtained the governing equation, boundary condition and initial condition for the transport coefficients ($K_n(\tau)$ and $f_n(\eta, \tau)$) of the Taylor–Gill generalized dispersion model. Thus, it is now possible

to solve $K_n(\tau)$ and $f_n(\eta, \tau)$ order by order. It is emphasized that the last term on the right-hand side of Eq. (26) is a summation which greatly increases the complexity of the solution procedure, with the inclusion of the wall absorption condition. Therefore, we do not solve Eq. (26) directly. Instead, we obtain $K_n$ *and* $f_n$ via their relationships with the moments of concentration distribution since this is much easier to solve. The solution procedure of $K_n(\tau)$ is exactly the same as that in Jiang and Chen [60]. We can follow §4 of Debnath *et al.* [61] to obtain the result of $K_n(\tau)$. For brevity, the detailed solution procedure is presented in appendix A. The main difference is that we have considered the microchannel flow and wall absorption at both walls in the present work. It turns out that a different eigenvalue problem for the concentration moments is needed to solve.

Here, we just write the final results of the mean concentration distribution. Following Debnath *et al.* [61], we also truncate Taylor–Gill expansion equation Eq. (24) at order three and thus the asymmetry of the mean concentration distribution (can be characterised by one of the non-Gaussian effects called skewness) can be captured. As discussed in §4 of Jiang and Chen[60] and §8 of Yu and Chang [62], the truncated model can be solved using the Fourier transformation. From Eq. (23) of Debnath *et al.*[61], we have,

$$\langle C\rangle = \frac{\langle M_0\rangle}{\left|\sqrt[3]{-3\omega_3}\right|}\exp\left(-\frac{\omega_2}{3\omega_3}\xi - \frac{\omega_1\omega_2}{3\omega_3} + \frac{2\omega_2^3}{27\omega_3^2}\right)^2 \mathrm{Ai}\left(\frac{-\xi-\omega_1+\frac{\omega_2^2}{3\omega_3}}{\sqrt[3]{3\omega_3}}\right) + \text{H.O.T.}, \tag{27}$$

where Ai is the *Airy function* of the first kind:

$$\mathrm{Ai}(\xi) = \frac{1}{2\pi}\int_{-\infty}^{\infty} \mathrm{e}^{\mathrm{i}(x\xi + x^3/3)}\,\mathrm{d}x, \tag{28}$$

and H.O.T. represents the higher-order terms. The coefficient $\omega_n$ is a function of time and its definition is

$$\omega_n(\tau) = \int_0^\tau K_n(\tau')\,\mathrm{d}\tau' \quad \text{for} \quad n = 0,1,2,\ldots. \tag{29}$$

## 4.VALIDATION WITH NUMERICAL SIMULATION

To validate the analytical results derived for the mean concentration distribution, the method of Brownian dynamics simulation (or numerical simulation of stochastic differential equations (SDEs)) is utilized. This method has a wide range of applications[63–66], especially for reaction–diffusion problems.

First, according to the relations between SDE and transport equation, the corresponding SDEs for the dimensionless governing equation (18a) of the transport in microchannel,

$$\mathrm{d}\xi = \mathrm{U}(\eta)\mathrm{d}\tau + \frac{\sqrt{2}}{\mathrm{Pe}}\mathrm{d}W_x, \tag{30a}$$

$$\mathrm{d}\eta = \sqrt{2}\mathrm{d}W_y, \tag{30b}$$

where $\xi(\tau)$ and $\eta(\tau)$ are the random horizontal and vertical coordinates of the particle. $W_x$ and $W_y$ are independent Brownian motions.

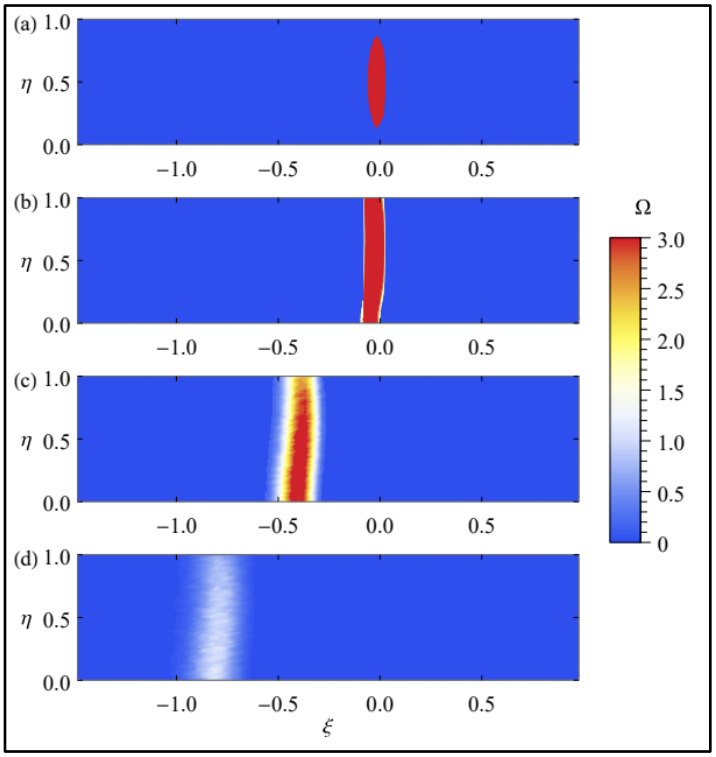


FIG. 3. Two-dimensional concentration distribution of the transport process by Brownian dynamics simulation at: (a) $\tau = 0.01$, (b) $\tau = 0.1$, (c) $\tau = 1$ and (d) $\tau = 2$. Parameters: $\psi_{\mathrm{wall}}^{12} = 0.5$, $\Gamma_0 = 0.1$, $\Gamma_1 = 1$, $\kappa = 10$, $\eta_0 = 0.5$ and $\mathrm{Pe} = 1000$.

In our simulations, the Euler–Maruyama method is applied to numerically solve the SDEs with a small enough time step $\Delta\tau = 10^{-3}$ (we have tested the time-step independence). In total, $5 \times 10^5$ solute particles are simulated. All of them are initially released at $\eta_0 = 0.5$ for the point-release initial condition. For the wall absorption in Eq. (18c), we follow Erban and Chapman [67], equation (10) to calculate the probability of absorption when a particle exceeds the wall after a time step during the simulation. Note that the absorption coefficients at the upper wall ($\eta = 1$) and at the lower wall ($\eta = 0$) can be different. For the upper wall, when a particle exceeds the wall ($\eta = 1$) at $n$-step simulation, i.e. $\eta_n > 1$, the probability $P_{a1}$ for the particle to be absorbed onto the wall is related to the absorption coefficient $\Gamma_1$ and

$$P_{a1} = \Gamma_1 \sqrt{\pi \Delta \tau}, \tag{31}$$

or it will be reflected back to the microchannel at a new transverse position of $\eta = 2 - \eta_n$. Analogously, for the lower wall ($\eta = 0$), when a particle exceeds the wall ($\eta_n < 0$), the absorptive probability $P_{a0}$ is

$$P_{a0} = \Gamma_0 \sqrt{\pi \Delta \tau}, \tag{32}$$

or the particle will be reflected back at $\eta = -\eta_n$. The absorption is irreversible and thus the absorbed particles will be removed in following simulations. The trajectories of all the particle motions are recorded and then are used to calculate the mean concentration distribution and other concentration statistics. Figure 3 shows the numerical result of the temporal evolution of the concentration distribution during the transport process for a specific case. The validation plot of the Brownian dynamics simulations against the Gill's generalized dispersion model for the mean concentration distribution is shown in Fig. 4 at two distinct times (a) $\tau = 1$ and (b) $\tau = 5$. The simulation parameters include $\Gamma_0/\Gamma_1 = 0.1$, $\kappa = 10$ and $\eta_0 = 0.5$. The numerical outcomes exhibit excellent agreement with the analytical predictions obtained through Gill's expansion procedure, confirming a robust correlation between the two methodologies. This alignment verifies the reliability and accuracy of the analytical techniques.

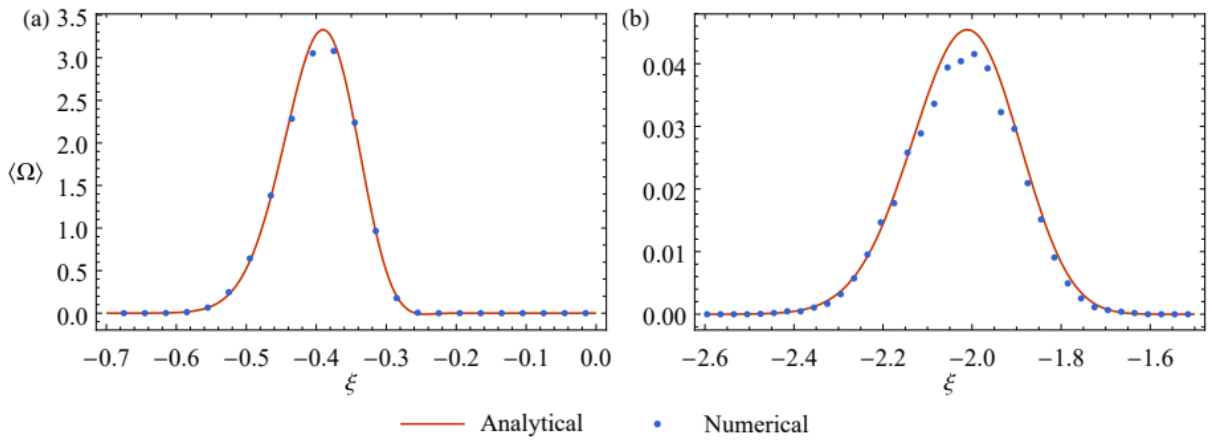


FIG. 4. Comparison of Brownian dynamics numerical solution for the mean concentration distribution with that obtained analytically by Gill's generalized dispersion model at: (a) $\tau = 1$ and (d) $\tau = 5$. Parameters: $\psi_{wall}^{12} = 0.5$, $\Gamma_0 = 0.1$, $\Gamma_1 = 1$, $\kappa = 10$, $\eta_0 = 0.5$ and Pe = 1000.

Figure 5 further displays the *long-time asymptotic values* of Gill's transport coefficients $K_n$ against $\Gamma_0/\Gamma_1$. Notably, the figure reveals a consistent functional relationship between the transport coefficient and the ratio of reaction rates, demonstrating a *decrease in all transport coefficients as the ratio of reaction rate constants increases*. This observed trend aligns with findings in existing literature, further validating the efficiency of Gill's series analytical approach.

## 5.RESULTS AND DISCUSSION

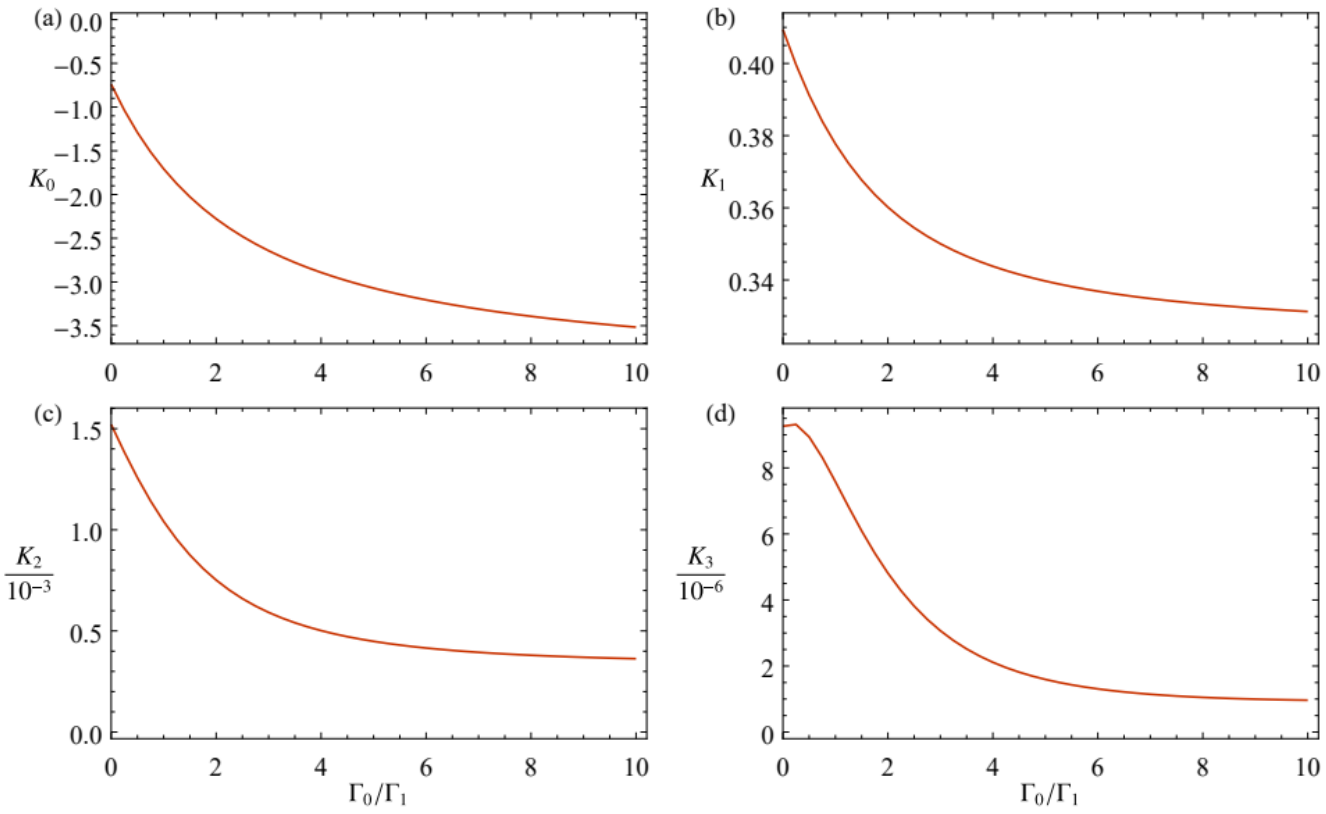


FIG. 5. The long-time asymptotic values of Gill's dispersion coefficients $K_n$ with different $\Gamma_0/\Gamma_1$. Other parameters: $\Gamma_1$ = 1, $\psi^{12}_{\text{wall}} = 0.5$, $\kappa$ = 10, $\eta_0$ = 0.5 and Pe = 1000.

In the present study, we scrutinize the intricacies of neutral solute transport within electro-osmotic flow in a microchannel. The primary focus is to *elucidate the consequences of point source solute injection on transport coefficients injected at various channel heights*. The point-source effect has been discussed for macroscopic flows such as wetland flows and open-channel flows[68–71], while the case of microchannel flows remains a need to investigate. To ascertain the mean concentration, we employ the third-order Gill series expansion technique with known values of transport coefficient obtained by the method of moment techniques, as shown in section III. Thus, the comprehensive analysis of the entire transport process is conducted by examining *four key transport coefficients*, viz., exchange coefficient ($K_0$), advection coefficient ($K_1$), dispersion coefficient ($K_2$) and asymmetry coefficient ($K_3$), respectively, as discussed in section VA. Then the mean concentration distribution is investigated in section VB.

In the present work, the solute dispersion is controlled by three key factors: *the reaction rate* (represented by $\Gamma_0/\Gamma_1$), *the thickness of the EDL* (represented by $\kappa$), and *the initial solute release position* (represented by $\eta_0$).

For simplicity of analysis, other parameters are assumed to be fixed without mentioned, including $\Gamma_1 = 1$, $Pe = 1000$ and $\psi_{\text{wall}}^{12} = 0.5$ (such that the flow in asymmetric with respect to the centerline of the microchannel).

## Transient behaviour of transport coefficient

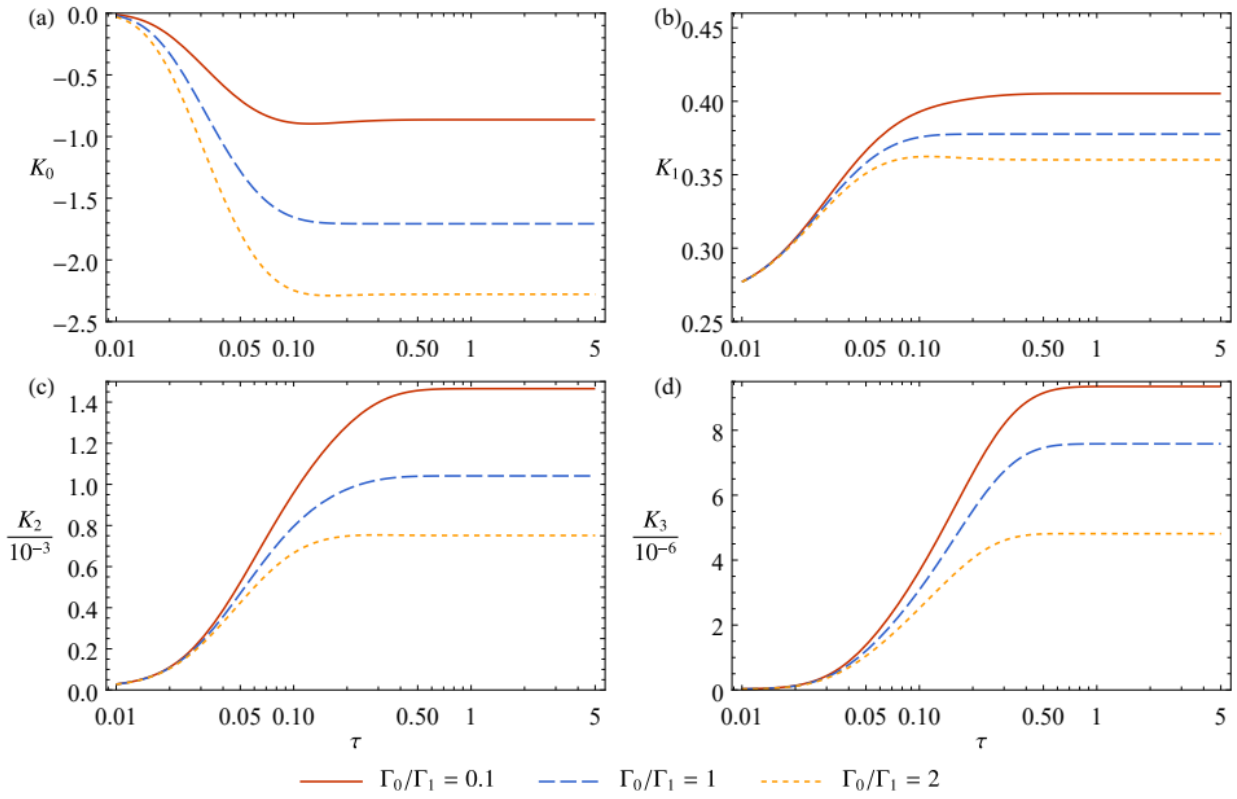


FIG. 6. Temporal evolution of Gill's dispersion coefficients $K_n$ with different reaction rate $\Gamma_0/\Gamma_1$. Fixed parameters: $\kappa = 10$ $\psi_{\text{wall}}^{12} = 0.5$, $\eta_0 = 0.5$.

Solute dispersion involves the spreading and mixing of a solute within a fluid medium. When the fluid medium is in motion, the spreading process initially depends on time, gradually stabilizing and becoming independent of time. This initial period of dispersion is known as the *transient solute dispersion regime*. The entire process is termed "unsteady solute dispersion". It is noteworthy that this transient solute dispersion phase is notably influenced by the initial conditions of the injected solute.

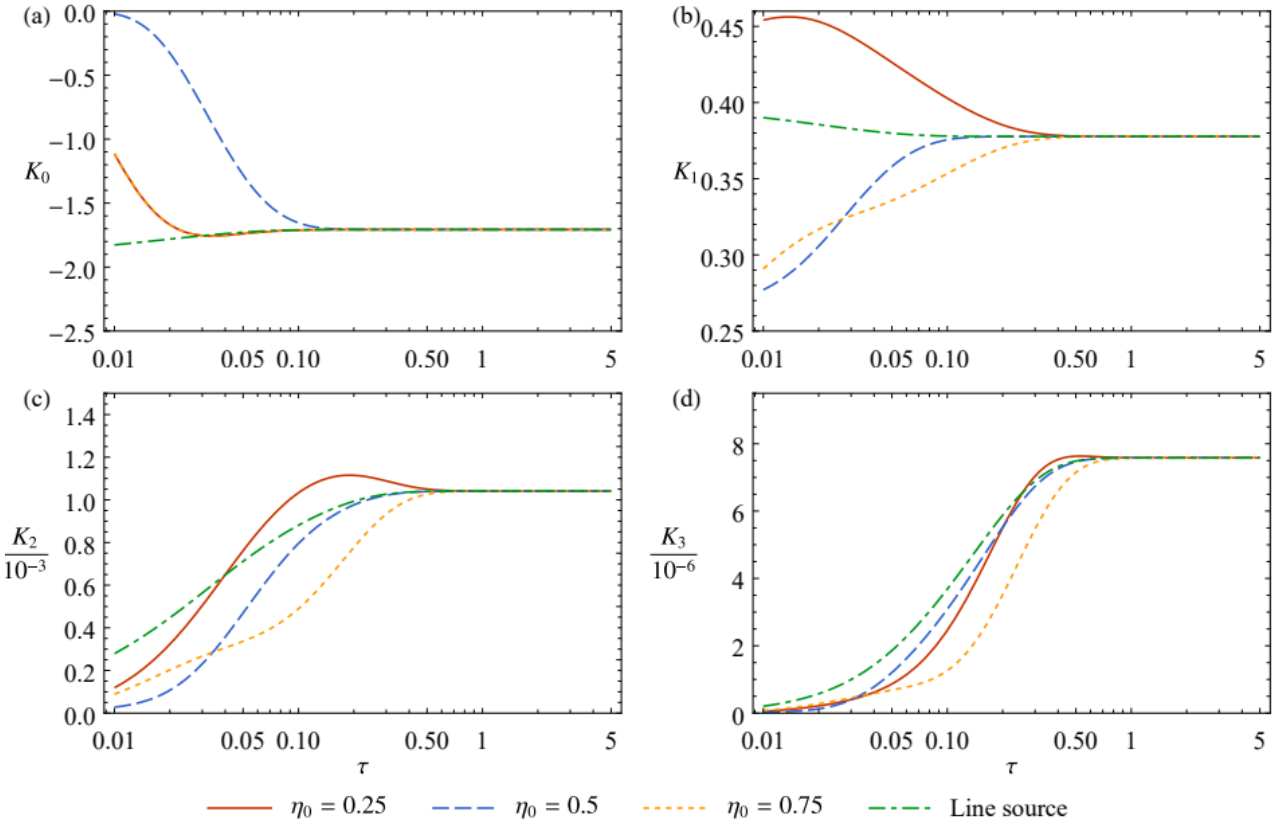


FIG. 7. Temporal evolution of Gill's dispersion coefficients $K_n$ for different initial conditions. The electro-osmotic flow is *asymmetric* with respect to the centerline of the microchannel with the ratio of wall electric potentials not equal to 1 (here, $\psi_{\text{wall}}^{12} = 0.5$). Other fixed parameters: $\Gamma_0/\Gamma_1 = 1$ and $\kappa = 10$.

In Fig. 6, all the evolution of all four transport coefficients is plotted against time to visualize the effect of reaction rate $\Gamma_0$ when $\kappa = 10$ and $\eta_0 = 0.5$. It is evident that as the ratio of the reaction rate constant increases, there is a noticeable rise in the magnitude of the exchange coefficient. This observed increase in the magnitude of the exchange coefficient with a higher ratio of reaction rate constant could be attributed to the intensified kinetics of the chemical reactions involved. A higher reaction rate constant implies a swifter progression of the chemical reactions responsible for the exchange process. This leads to an escalation in the magnitude of exchange coefficient. Figure 6(b) depicts the transient distributions of the advection coefficient $K_1$ (which is related to the average velocity of the carrier fluid) with variation in reaction rate $\Gamma_0/\Gamma_1$ (because we have assumed $\Gamma_1 = 1$ as a fixed parameter). It is noted that advection coefficient is enhanced with time and tends towards a uniform state. If we increase the reaction rate, the value of $K_1$ displays a decaying nature, though the difference of magnitudes is not excessive. Apparently as the reaction rate increases, the impact on the fluid velocity is less pronounced, resulting in a comparatively modest change in the advection

coefficient. Among all the transport coefficients, the dispersion coefficient is the key parameter in the context of describing the spreading of solutes due to the *combined action of convection, axial and radial diffusion*.

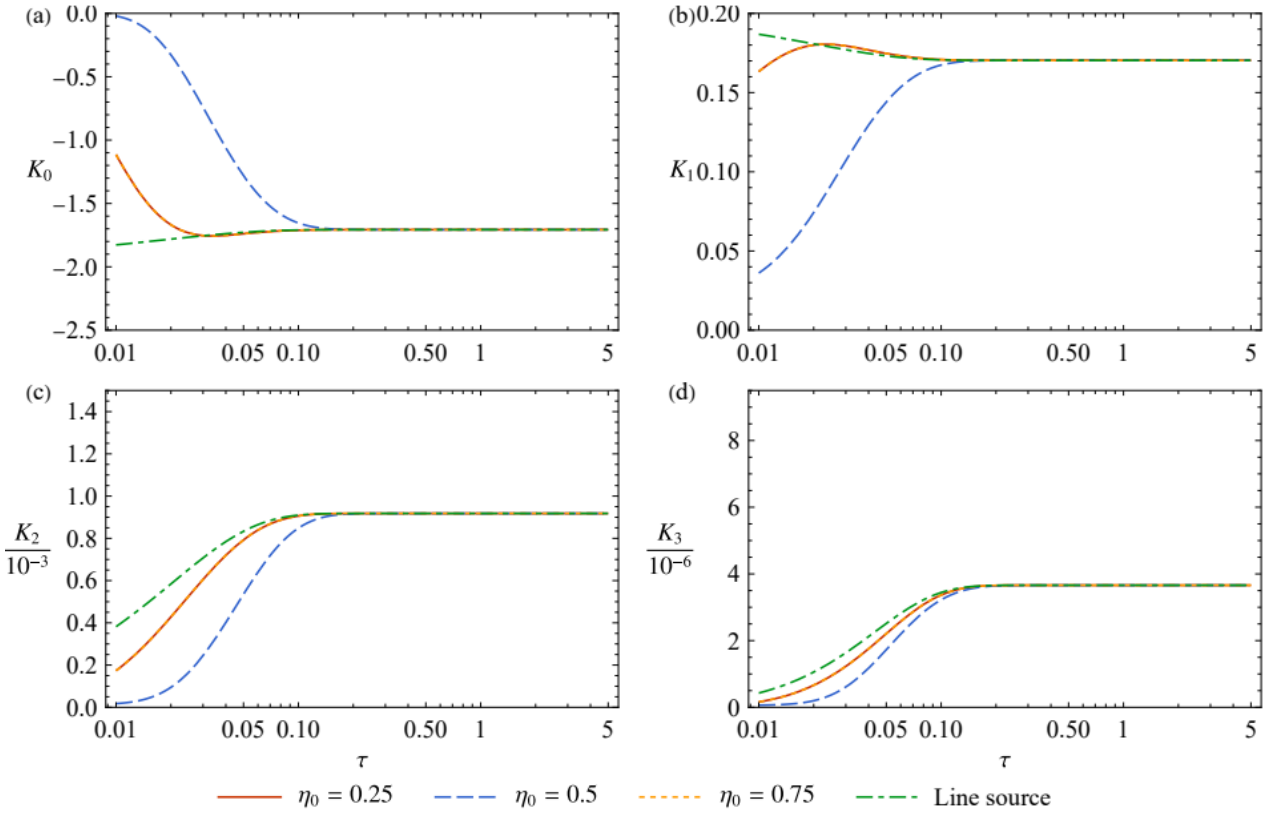


FIG. 8. Temporal evolution of Gill's dispersion coefficients $K_n$ for different initial conditions. The electro-osmotic flow is *symmetric* with respect to the centerline of the microchannel (i.e., the ratio of wall electric potentials, $\psi_{\text{wall}}^{12} = 0.5$). Other fixed parameters: $\Gamma_0/\Gamma_1 = 1$ and $\kappa = 10$.

Figure 6(c) shows the dispersion coefficient ($K_2$) versus time with various reaction rate values. As anticipated, the magnitude of the dispersion coefficient decreases with the reaction rate. This has been observed in a number of other studies[46,48–52]. A similar pattern is also computed in Fig. 6(d). In Fig. 6(d) an attempt has also been made to capture the *flow asymmetry*. It is evident that as the reaction rate rises, asymmetry coefficient, $K_3$ tends to zero more quickly than when the reaction rate is smaller. In other words, depending on the reaction rate, flow symmetry can be reached quickly. It is also pertinent to mention that in previous studies [27-29, 46] we have observed that $K_2$ (dispersion coefficient) does indeed converge to Taylor's classical limit at high Péclet numbers. However, for brevity we have not explored this aspect in the current study.

In Fig. 7, the temporal variation of transport coefficients is shown for various values of the *initial solute release position* ($\eta_0$) along with the release of line source solute. We can see that when the release position

is located at $\eta_0 = 0.25$, the magnitude of $K_0$ is greater than for the case when $\eta_0 = 0.5$. Also, the time necessary to attain the uniform state is faster if the release position is at $\eta_0 = 0.25$. Importantly, here both the wall reaction rates are assumed to be same. Thus, the value of $K_0$ coincides when the release position is at $\eta_0 = 0.75$. In all three cases of $\eta_0$, *it is clear if the release position is in closer proximity to the wall and since the microchannel walls react chemically with the solute*, the equilibrium state is achieved more quickly. Further, the line source exhibits a much faster exchange rate between the inter-phases. For the case of advection coefficient $K_1$, we have observed an opposite nature of spreading at the different solute release positions (Fig. 7(b)).

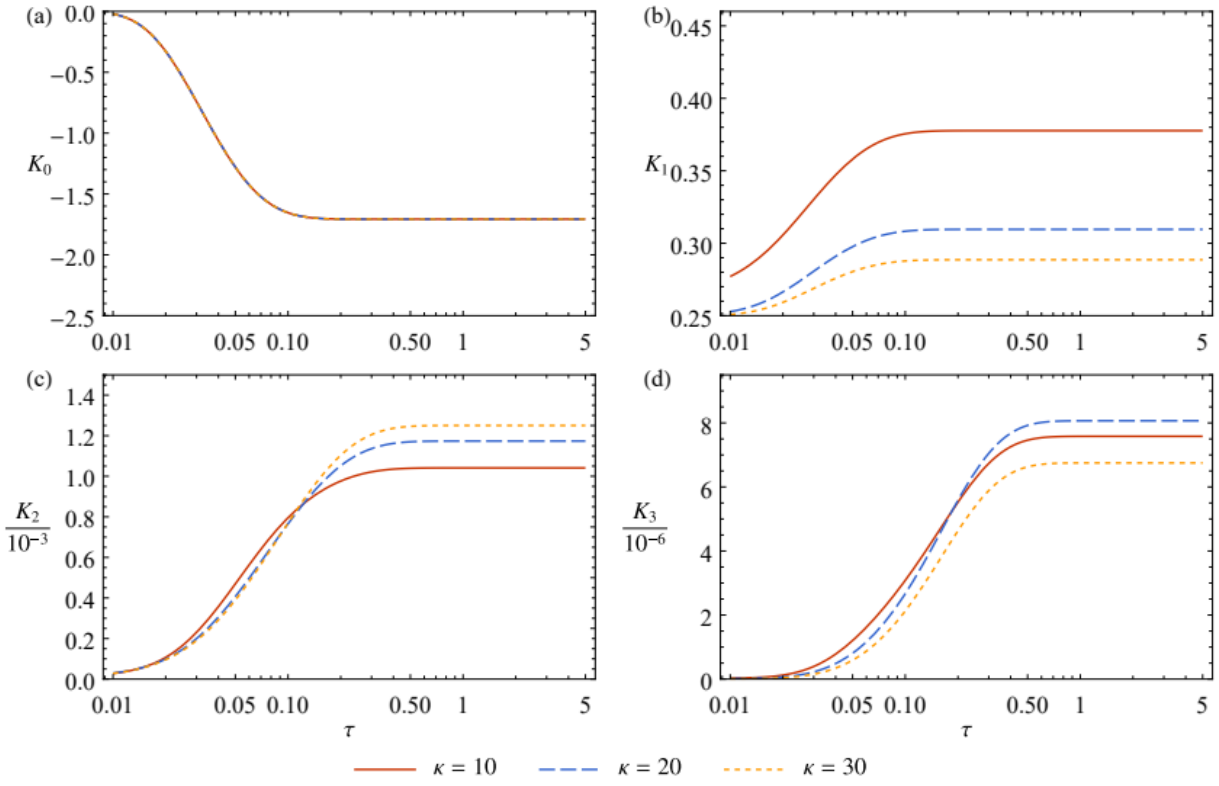


FIG. 9. Temporal evolution of Gill's dispersion coefficients $K_n$ for different Debye–Hückel parameter values $\kappa$. The electro-osmotic flow is *asymmetric* with respect to the centerline of the microchannel ($\psi_{wall}^{12} = 0.5$). Other fixed parameters: $\Gamma_0/\Gamma_1 = 1$ and $\eta_0 = 0.5$.

The advection coefficient shows an increasing trend with time at a release position $\eta_0 = 0.75$; whereas there is a decreasing trend when $\eta_0 = 0.25$. However, after a fixed time both the curves find a common point of interaction. This may explain the asymmetric flow profile due to different wall electrical potentials. Considering the dispersion coefficient in Fig. 7(c), we have observed a transient anomalous diffusion computed at different release positions. The value of dispersion coefficient demonstrates an increasing nature

with time for all the cases of solute release and finally reaches the classical Taylor limit. Therefore, in this small interval of time the distribution will be *highly skewed*, which is clearly observed from Fig. 7(d). It must be emphasized that the nature of transport coefficients due to solute release at two symmetric locations in the channel contributes to the asymmetric flow profile when $\psi_{\text{wall}}^{12} = 0.5$. In Fig. 8, this pattern is visualized for a symmetric flow profile with $\psi_{\text{wall}}^{12} = 1$. The plots reveal that all the dispersion coefficients converge asymptotically to the steady state at large values of time ($\tau$). While $K_o$ coefficient (Fig 8a) descends from a maximum at initial time, the other coefficients i.e. $K_1$, $K_2$ and also $K_3$ (Figs. 8b, c, d) clearly ascend from a minimum magnitude at initial time, to climb to the higher asymptotic value computed at the steady state, for larger time (i.e. Taylor's classical limit). Therefore, while different topologies of the coefficient profiles are computed through time, the ultimate fate is the same, with a plateau distribution achieved in the steady state, as originally observed by Taylor [14, 15].

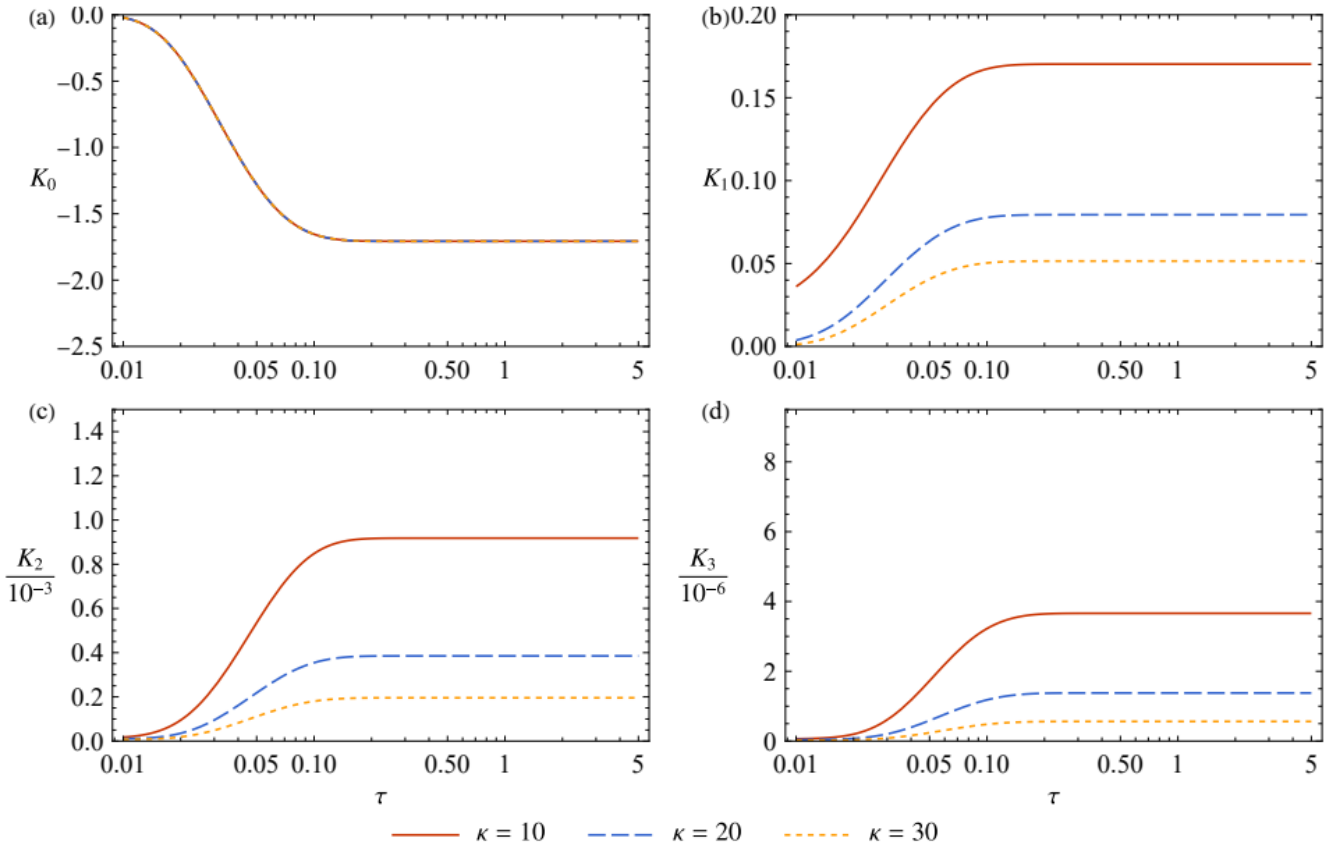


FIG. 10. Temporal evolution of Gill's dispersion coefficients $K_n$ for different Debye–Hückel parameter values $\kappa$. The electro-osmotic flow is *symmetric* with respect to the centerline of the microchannel ($\psi_{\text{wall}}^{12} = 1$). Other fixed parameters: $\Gamma_0/\Gamma_1 = 1$ and $\eta_0 = 0.5$.

In Figs. 9 and 10, the influe nce of Debye–Hückel parameter ($\kappa$) is plotted for all the four transport coefficients, with an asymmetric electro-osmotic flow ($\psi_{\text{wall}}^{12} = 0.5$ in Fig. 9) and with a symmetric flow ($\psi_{\text{wall}}^{12} = 0.5$ in Fig. 10). The EDL thickness is controlled by the parameter $\kappa$. As the value of $\kappa$ increases, the EDL thickness decreases. No tangible modification is observed in the exchange coefficient $K_0$ with time (Fig. 9(a) and Fig. 10(a)) with an increment in $\kappa$ when $\psi_{\text{wall}}^{12} = 0.5$ and 1. It is evident from Eq. (24) that $K_0$ is *only affected by the wall reaction.* However, as $\kappa$ rises the value of advection coefficient $K_1$ is modified and clearly decreases (Fig. 9(b) and Fig. 10(b)). As the value of $\kappa$ increases the time taken by $K_1$ to achieve the steady state is also decreased.

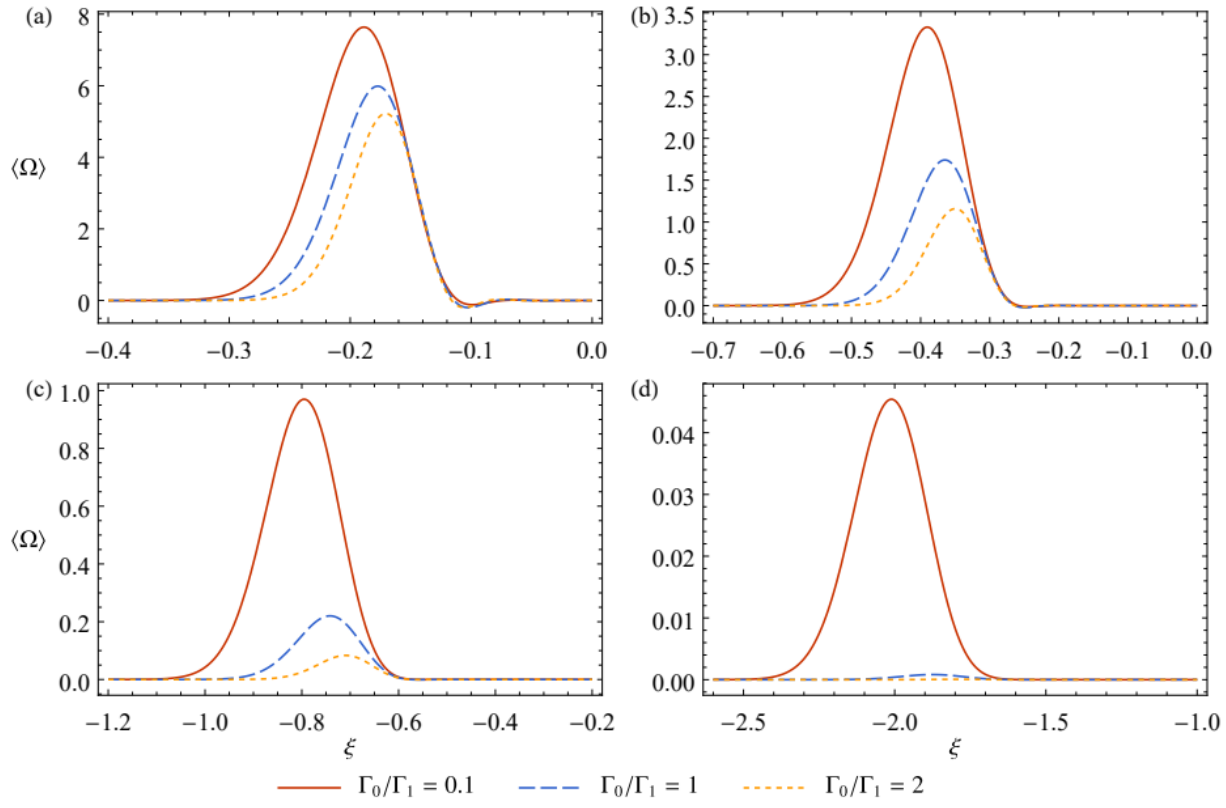


FIG. 11. Longitudinal distribution of the cross-sectional average concentration for different $\Gamma_0/\Gamma_1 = 1$ at: (a) $\tau = 0.5$, (b) $\tau = 1$, (c) $\tau = 2$ and (d) $\tau = 5$. Other fixed parameters: $\kappa = 10$, $\eta_0 = 0.5$ and $\Gamma_1 = 1$.

An interesting result can be seen from Fig. 9(c) and Fig. 10(c) for the case of the dispersion coefficient, ($K_2$). The magnitude of the dispersion coefficient is enhanced with time for any value of $\kappa$ irrespective of the wall potential ratio. However, the value of the dispersion coefficient exhibits an anomalous trend with Debye–Hückel parameter $\kappa$ due to the ratio of wall potentials $\psi_{\text{wall}}^{12} = 0.5 = 0.5$ and 1. When $\psi_{\text{wall}}^{12} = 0.5$, in a smaller interval of time the value of the dispersion coefficient suppressed with time for larger values of κ;

however, after further elapse in time, a reverse pattern is computed. Conversely, a consistently uniform distribution in the dispersion coefficient is computed for all time when the wall potentials are equal. In Fig. 9(c) and Fig. 10(c), the temporal variation of the asymmetry coefficient with various $\kappa$ is observed. Different $\psi_{\text{wall}}^{12}$values do not exert any substantial change effectively on the asymmetry coefficient. However, it is evident that the Gaussian distribution curve may be achieved faster for larger κ and furthermore when the electrical potentials at both the microchannel walls are the same.

## Longitudinal distribution of the cross-sectional average concentration

The longitudinal distribution of solute mean concentration is studied with the aid of Figs. 11 to 13, under various conditions. All the figures are drawn for four distinct times, $\tau = 0.5$, $\tau = 1$, $\tau = 2$ and $\tau = 5$, respectively. Here, we only consider the case of an asymmetric electro-osmotic microchannel flow with the wall potential ratio $\psi_{\text{wall}}^{12} = 0.5$. The influences of the reaction rate ratio, the thickness of the EDL, and the initial solute release position are discussed sequentially.

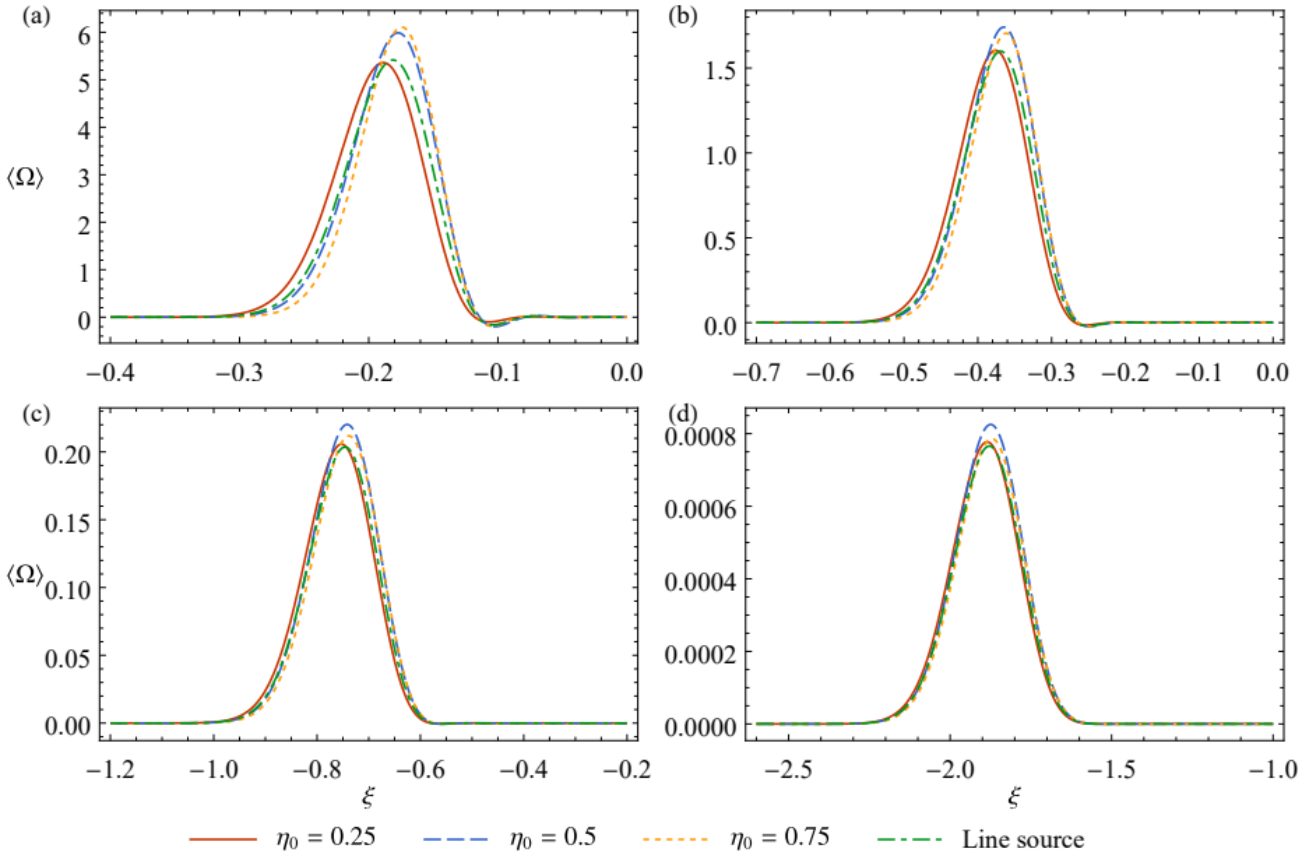


FIG. 12. Longitudinal distribution of the cross-sectional average concentration for different initial conditions at: (a) τ = 0.5, (b) τ = 1, (c) τ = 2 and (d) τ = 5. Other fixed parameters: $\Gamma_0/\Gamma_1 = 1$ and $\kappa = 10$

First, for the reaction rate ratio $\Gamma_0/\Gamma_1$, when $\kappa$ = 10 and $\eta_0$ = 0.5, Fig. 11 shows that the peak of the concentration curve diminishes with increasing reaction rate for all cases. Additionally, as time progresses, the overall magnitudes of the distribution curve are depleted significantly. The solute distribution slowly morphs towards the Gaussian normal curve with elapse in time. The results for the influence of reaction rate on concentration distribution confirm those observed in many previous studies including the papers of Sadeghi *et al.* [47] and Roy *et al.*[46]

In Fig. 12, the mean concentration profiles for different release positions with respect to time are illustrated for different initial conditions (solute release positions). The results are drawn for fixed values of $\Gamma_0/\Gamma_1$ = 1 and $\kappa$ = 10. It can be seen that for $\tau$ = 0.5 and 1, the height of the mean concentration distribution increases with $\eta_0$. Even though the release positions $\eta_0$ = 0.25 and $\eta_0$ = 0.75 are symmetric in the microchannel, nevertheless, the concentration profiles are distinct due to the asymmetric velocity effects (with different wall potential $\psi_{\text{wall}}^{12} = 0.5$). However, these scenarios change at times $\tau$ = 2 and $\tau$ = 5. As time increases, it is evident that the difference of mean concentration profiles for $\eta_0$ = 0.5 and 1 slowly tend towards the same value (see Fig. 12(c,d)).

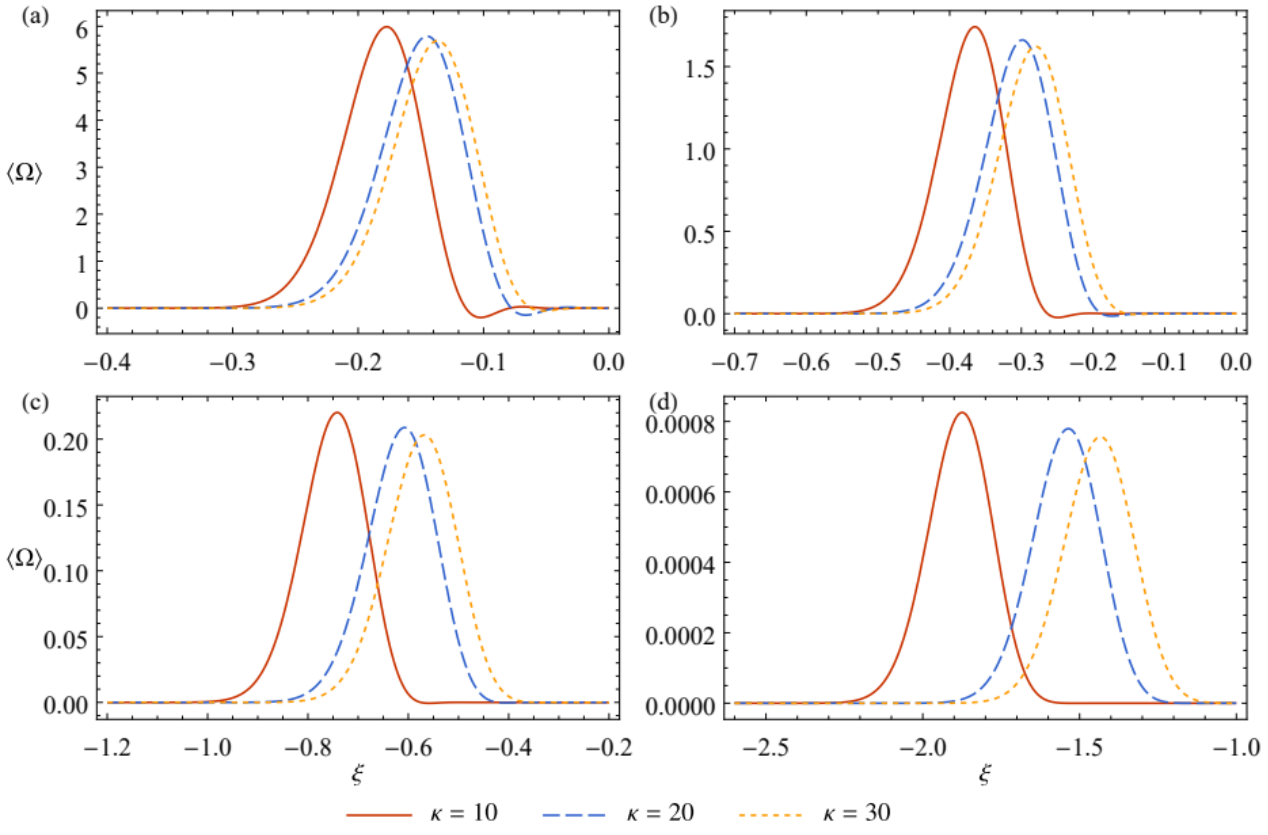

FIG. 13. Longitudinal distribution of the cross-sectional average concentration for different $\kappa$ at: (a) $\tau$ = 0.5, (b) $\tau$ = 1, (c) $\tau$ = 2 and (d) $\tau$ = 5. Other fixed parameters: $\Gamma_0/\Gamma_1$ = 1 and $\eta_0$ = 0.5.

In Fig. 13, we have studied the axial mean concentration distribution due to the effect of Debye–Hückel parameter, $\kappa$. The plots are similar to previous figures when $\Gamma_0/\Gamma_1$ = 1, $\psi_{\text{wall}}^{12} = 0.5$ and $\eta_0$ = 0.5. In all the cases the value of $\kappa$ reduces the mean concentration distribution axially.

## 6.CONCLUSIONS

As a simulation of a bio-microfluidic device, a theoretical and numerical study has been presented for the generalized Taylor–Gill electro-kinetic hydrodynamic dispersion of a point source solute injected in a microchannel, under constant axial static electric field and different charged surface wall potentials. The solute is assumed to obey a first-order irreversible absorptive chemical reaction at both the channel walls with different absorptive coefficients The solute transport phenomena are simulated using a modified electrokinetic unsteady convective diffusion equation. Employing Gill's concentration decomposition technique up to third-order accuracy, a detailed analysis of the entire transport process has been conducted. Furthermore, a comprehensive comparison between analytical outcomes and numerical simulations using the Brownian Dynamics method has been included. The focus has been the influence of electrokinetic, reaction and solute position effects on evolution in the four key transport coefficients i.e., *exchange, advection, dispersion and asymmetry coefficients, along with the mean concentration profile.* The computations have shown that:

**i)** The location of the initial solute release at various heights of the microchannel has a considerable impact on all the transport coefficients.

**ii)** Peak longitudinal concentration is reduced with increasing reaction rate and as time progresses, the overall magnitudes of the distribution curve are depleted significantly.

**iii)** The solute distribution slowly morphs towards the Gaussian normal curve with elapse in time.

**iv)** The magnitude of the dispersion coefficient is elevated with time for any value of Debye– Hückel parameter irrespective of the wall potential ratio.

**v)** Exchange coefficient, $K_0$ is only affected by the wall reaction. However, as $\kappa$ rises, the value of advection coefficient $K_1$ is modified and clearly decreases (Fig. 9(b) and Fig. 10(b)). As the value of $\kappa$ increases, the time taken by $K_1$ to achieve the steady state is also decreased.

**vi)** The advection coefficient shows an increasing trend with time at larger values of solute release position

($\eta_0 = 0.75$) compared to a decreasing trend at lower values ($\eta_0 = 0.25$).

**vii)** The value of dispersion coefficient ($K_2$) demonstrates an increasing nature with time for all the cases of solute release and finally reaches the classical Taylor limit. Dispersion coefficient ($K_2$) decreases with absorptive reaction rate.

**viii)** Asymmetry coefficient ($K_3$) approaches zero more quickly than when the reaction rate is smaller i.e., depending on reaction rate, flow symmetry can be reached quickly.

The present study has revealed some interesting characteristics of electrokinetic hydro- dynamic dispersion in micro-conduits using both analytical Gill decomposition expansion and Brownian dynamics computational methods. However, attention has been confined to Newtonian ionic liquids and has neglected and electrolytic property variation and variable zeta potential.

## ACKNOWLEDGMENTS

This work is supported by the Science and Technology Development Fund (FDCT) of Macao SAR (Project Nos. 0018/2023/ITP1, 0041/2021/AGJ, and 001/2022/NIF) and the National Natural Science Foundation of China (Grant No. 52109093). All the authors are grateful to both reviewers for their excellent comments which have served to improve the clarity of the work.

## CONFLICT OF INTEREST

The authors declare no potential conflict of interest.

## Appendix A: Solve the transport coefficients by the concentration moment method.

### 1. Relationship between transport coefficients and cumulants

Here, we follow §4 of Debnath *et al.* [61] and solve the transport coefficients $K_n(\tau)$ using the method of concentration moments. $K_n(\tau)$ can be expressed in terms of concentration moments (or cumulants), whose governing equation of concentration moments is much more straightforward to solve.

First, the definition $n^{th}$ order concentration moment (following Aris [17]) is:

$$M_n(\xi,\tau)=\int_{-\infty}^{\infty}\xi^n\Omega(\xi,\eta,\tau)\,\mathrm{d}\xi,\ \text{for}\ n=0,1,\ldots. \tag{A1}$$

Analogously, the *n*-th order moment of the cross-sectional mean concentration

$$\bar{M}_n(\tau)=\int_{-\infty}^{\infty}\xi^n\bar{\Omega}\,\mathrm{d}\xi=\langle M_n\rangle, \tag{A2}$$

where we have used a bar to denote the variables related to the mean concentration distribution $\bar{\Omega}=\langle\Omega\rangle$. Note that $\Omega$ and $\bar{\Omega}$ may not be well-defined probability density functions (PDFs) because of the wall absorption. To obtain the statistical raw moments and cumulants, normalization is required,

$$P(\xi,\eta,\tau)=\frac{\Omega(\xi,\eta,\tau)}{M_0(\eta,\tau)},\quad \bar{P}(\xi,\tau)=\frac{\bar{\Omega}(\xi,\tau)}{\bar{M}_0(\tau)}. \tag{A3}$$

Notice that $\bar{P}$ might not equal to $\langle P\rangle$. Now $P$ and $\bar{P}$ are PDFs and we can safely calculate their statistics. Here, we just show $\bar{P}$ as an example. The *n*-th raw moment $\bar{\mu}_n'$ is

$$\bar{\mu}_n'(\tau)=\int_{-\infty}^{\infty}\xi^n\bar{\Omega}(\xi,\tau)\,\mathrm{d}\xi=\frac{\bar{M}_n}{\bar{M}_0}, \tag{A4}$$

The first few cumulants are defined as[72–74]

$$\bar{\chi}_1=\bar{\mu}_1',\quad \bar{\chi}_2=\bar{\mu}_2'-\bar{\mu}_1'^2,\quad \bar{\chi}_3=\bar{\mu}_3'-3\bar{\mu}_2'\bar{\mu}_1'+2\bar{\mu}_1'^3. \tag{A5}$$

Here, $\chi$ is used to denote the cumulant instead of the convectional symbol $\kappa$ because we have used $\kappa$ for the EDL length.

Finally, we express the transport coefficients $K_n(\tau)$ with the cumulants. Details can be found in §5 of Frankel and Brenner[75] and §3 of Jiang and Chen[60] with the help of Fourier transform. For the exchange coefficient,

$$K_0=\frac{\mathrm{d}}{\mathrm{d}\tau}\ln\bar{M}_0. \tag{A6}$$

For $K_n$ with $n..1$,

$$K_n(\tau) = \frac{(-1)^n}{n!}\frac{\mathrm{d}\bar{\chi}_n(\tau)}{\mathrm{d}\tau}. \tag{A7}$$

## 2. Eigenvalue problem of the concentration moments

The remained problem is the solution of concentration moments. Fortunately, one can easily apply the method of separation of variables to solve them (or use the integral trans- formation technique[76]), following the approach described by Aris [17]. Barton [77] even provided the solution expressions in a general format with undetermined eigenvalues and eigenfunctions. Therefore, the focus is to address the eigenvalue problem considering wall absorption at both channel walls. Note that the current eigenvalue problem is fundamentally different from that discussed in Debnath *et al.*[61], who considered the case in a tube flow.

First, we derive the governing equation of concentration moments. It is assumed that concentration decays exponentially as $|x| \to \infty$ (cf. Aris [17]). Integrating Eq. (18a) of con- centration, we have

$$\frac{\partial M_n}{\partial \tau} = \frac{\partial^2 M_n}{\partial \eta^2} + n\mathrm{U}M_{n-1} + \frac{n(n-1)}{Pe^2}M_{n-2}, \tag{A8}$$

where $M_{-1} = M_{-2} = 0$ (auxiliary terms) and $n = 0,1,\ldots$.

The corresponding absorptive boundary conditions at the microchannel walls are

$$\frac{\partial M_n}{\partial \eta} = \begin{cases} -\Gamma_1 M_n & \text{at } \eta = 1, \\ \Gamma_0 M_n & \text{at } \eta = 0, \end{cases} \tag{A9}$$

The transport problem with absorption at both walls has been investigated by some studies[53–56]. However, they have applied the multi-time scale homogenization technique and thus the eigenvalue problem with absorption at both walls not available in these papers. For- tunately, this kind of eigenvalue problem has been discussed in the textbook by Polyanin[78], p. 283 and thus we can directly use the solutions therein.

In the current notation, the whole associated eigenvalue problem for the concentration moments (A8) is

$$\frac{\partial^2 f}{\partial \eta^2} = -\lambda f, \tag{A10a}$$

$$\frac{\partial f}{\partial \eta} = \begin{cases} -\Gamma_1 f & \text{at } \eta = 1, \\ \Gamma_0 f & \text{at } \eta = 0, \end{cases}, \tag{A10b}$$

where $\lambda = \rho^2$ is the eigenvalue and $f(\eta)$ is the associated eigenfunction. The solution of $f(\eta)$ is

$$f(\eta) = A\cos(\rho\eta) + B\sin(\rho\eta), \tag{A11}$$

where $A$ and $B$ are undetermined coefficients for normalization, and we have $\rho B = \Gamma_0 A$ according to boundary condition at $\eta = 0$. Using the boundary condition at $\eta = 1$, we obtain the transcendental equation for the eigenvalue,

$$(\Gamma_0 + \Gamma_1)\rho = (\rho^2 - \Gamma_0\Gamma_1)\tan\rho \tag{A12}$$

This leads to a discrete set of eigenvalues $\{\lambda_m\}_{m=1}^{\infty}$ and their corresponding eigenfunctions $\{f_m(\eta)\}_{m=1}^{\infty}$. Finally, the solution of $M_n$ can be obtained by the orthogonal expansion:

$$M_n(\eta,\tau) = \sum_{m=1}^{\infty} \alpha_{nm}(\tau) f_m(\eta). \tag{A13}$$

The detailed solutions of coefficients $\alpha_{nm}(\tau)$ can be found in the work of Wang and Chen [79] and Yang *et al.* [80]. Here, we truncate the series using the first 10 eigenvalues and eigen- functions for the summation. Figure 14 shows that the analytical result of concentration moments and cumulants is in good agreement with the numerical result obtained by the Brownian dynamics simulation employed in section IV.

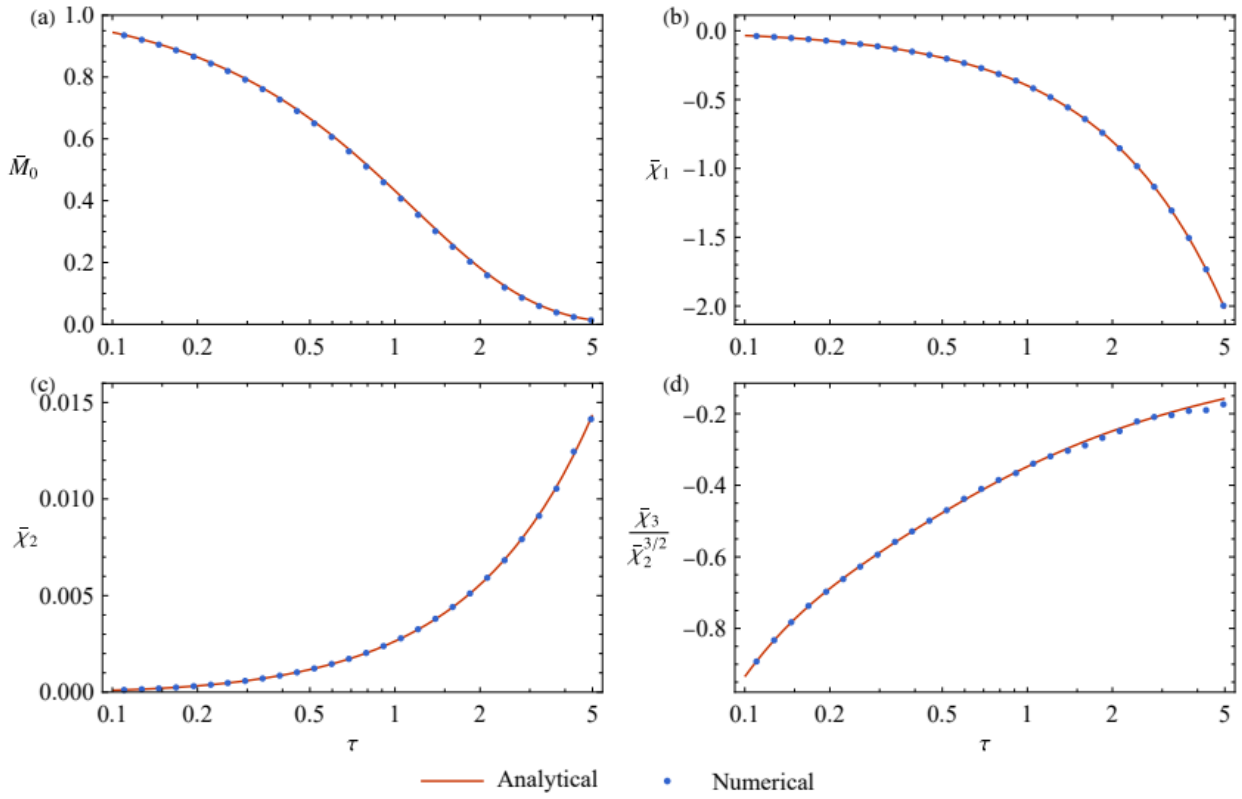


FIG. 14. Comparison of numerical result of Brownian dynamics simulation with the analytical solution for mean concentration moments and cumulants: (a) zeroth-order moment $\bar{M}_0$, (b) the first cumulant (the mean) $\bar{\chi}_1$, (c) the second cumulant (the variance) $\bar{\chi}_2$, and (d) skewness Parameters $\frac{\bar{\chi}_3}{\bar{\chi}_2^{3/2}}$. $\psi_{\text{wall}}^{12} = 0.5$, $\Gamma_0 = 0.1$, $\Gamma_1 = 1$, $\kappa = 10$, $\eta_0 = 0.5$ and $Pe = 1000$.

## REFERENCES

[1]C. Gandolfi, A. Facchi, and M. J. Whelan, "On the relative role of hydrodynamic dispersion for river water quality," Water Resour. Res. **37**, 2365–2375 (2001).

[2]L. Zeng, Y. H. Wu, P. Ji, B. Chen, Y. J. Zhao, G. Q. Chen, and Z. Wu, "Effect of wind on contaminant dispersion in a wetland flow dominated by free-surface effect," Ecol. Modell. **237–238**, 101–108 (2012).

[3]P. Wang and G. Q. Chen, "Contaminant transport in wetland flows with bulk degradation and bed absorption," J. Hydrol. **552**, 674–683 (2017).

[4]J. Guo, W. Jiang, and G. Chen, "Transient solute dispersion in wetland flows with sub- merged vegetation: an analytical study in terms of time-dependent properties," Water Resour. Res. **56**, e2019WR025586 (2020).

[5]M. Y. Guan, L. Zeng, W. Q. Jiang, X. L. Guo, P. Wang, Z. Wu, Z. Li, and G. Q. Chen, "Effects of wind on transient dispersion of active particles in a free-surface wetland flow," Commun. Nonlinear Sci. Numer. Simul. **115**, 106766 (2022).

[6]V. Prigiobbe, M. A. Hesse, and S. L. Bryant, "Fast strontium transport induced by hydrodynamic dispersion and pH-dependent sorption," Geophys. Res. Lett. **39** (2012), 10.1029/2012gl053146

[7]A. Ajdari, N. Bontoux, and H. A. Stone, "Hydrodynamic dispersion in shallow microchannels: The effect of cross-sectional shape," Anal. Chem. **78**, 387–392 (2006).

[8]L. Jofre and J. Urzay, "Interface dynamics in the transcritical flow of liquid fuels into high- pressure combustors," in *53rd AIAA/SAE/ASEE Joint Propulsion Conf.* (AIAA, Atlanta, GA, 2017).

[9]H. A. Kooijman and R. Taylor, "Estimation of diffusion coefficients in multicomponent liquid systems," Ind. Eng. Chem. Res. **30**, 1217–1222 (1991).

[10]W. Jiang and G. Chen, "Dispersion of active particles in confined unidirectional flows," J. Fluid Mech. **877**, 1–34 (2019).

[11]B. Wang, W. Jiang, and G. Chen, "Dispersion of a gyrotactic micro-organism suspension in a vertical pipe: the buoyancy–flow coupling effect," J. Fluid Mech. **962**, A39 (2023).

[12]A. K. Roy and O. A. Bég, "Asymptotic study of unsteady mass transfer through a rigid artery with multiple irregular stenoses," Appl. Math. Comput. **410**, 126485 (2021).

[13]H. Brenner and D. A. Edwards, *Macrotransport Processes* (Butterworth-Heinemann, Stoneham, MA, USA, 1993).

[14]G. I. Taylor, "Dispersion of soluble matter in solvent flowing slowly through a tube," Proc. R. Soc. A **219**, 186–203 (1953).

[15]G. I. Taylor, "Conditions under which dispersion of a solute in a stream of solvent can be used to measure molecular diffusion," Proc. R. Soc. A **225**, 473–477 (1954).

[16]M. Guan and G. Chen, "Streamwise dispersion of soluble matter in solvent flowing through a tube," J. Fluid Mech. **980**, A33 (2024).

[17]R. Aris, "On the dispersion of a solute in a fluid flowing through a tube," Proc. R. Soc. A **235**, 67–77

(1956).

[18]W. N. Gill and R. Sankarasubramanian, "Exact analysis of unsteady convective diffusion," Proc. R. Soc. A **316**, 341–350 (1970).

[19]W. N. Gill and R. Sankarasubramanian, "Dispersion of a non-uniform slug in time- dependent flow," Proc. R. Soc. A **322**, 101–117 (1971).

[20]E. J. Watson, "Diffusion in oscillatory pipe flow," J. Fluid Mech. **133**, 233–244 (1983).

[21]S. B. Hazra, A. S. Gupta, and P. Niyogi, "On the dispersion of a solute in oscillating flow through a channel," Heat Mass Transf. **31**, 249–256 (1996).

[22]L. Zeng, G. Q. Chen, Z. Wu, Z. Li, Y. H. Wu, and P. Ji, "Flow distribution and environmental dispersivity in a tidal wetland channel of rectangular cross-section," Commun. Nonlinear Sci. Numer. Simul. **17**, 4192–4209 (2012)

[23]Z. Wu, L. Zeng, G. Q. Chen, Z. Li, L. Shao, P. Wang, and Z. Jiang, "Environmental dispersion in a tidal flow through a depth-dominated wetland," Commun. Nonlinear Sci. Numer. Simul. **17**, 5007–5025 (2012).

[24]C.-O. Ng, "Dispersion in steady and oscillatory flows through a tube with reversible and irreversible wall reactions," Proc. R. Soc. A **462**, 481–515 (2006).

[25]G. R. Kiran, G. Radhakrishnamacharya, and O. A. Bég, "Peristaltic flow and hydro- dynamic dispersion of a reactive micropolar fluid-simulation of chemical effects in the digestive process," J. Mech. Med. Biol. **17**, 1750013 (2017).

[26]A. K. Roy and O. A. Bég, "Mathematical modelling of unsteady solute dispersion in two-fluid (micropolar-Newtonian) blood flow with bulk reaction," Int. Commun. Heat Mass Transfer **122**, 105169 (2021).

[27]A. K. Roy, O. A. Bég, A. K. Saha, and J. V. R. Murthy, "Taylor dispersion in non-Darcy porous media with bulk chemical reaction: a model for drug transport in impeded blood vessels," J. Eng. Math. **127**, 24 (2021).

[28]O. A. Bég and A. K. Roy, "Moment analysis of unsteady bi-component species (drug) transport with

coupled chemical reaction in non-Newtonian blood flow," Chin. J. Phys. **77**, 1810–1826 (2022).

[29]S. Debnath, A. K. Roy, and O. A. Bég, "Reactive solute transport in blood flow through a permeable capillary," Arch. Mech. **74**, 173–200 (2022).

[30]N. Hu, Y. Ai, and S. Qian, "Field effect control of electrokinetic transport in micro/nanofluidics," Sens. Actuators B Chem. **161**, 1150–1167 (2012).

[31]K. B. S. Latha, M. G. Reddy, D. Tripathi, O. A. Bég, S. Kuharat, H. Ahmad, D. U. Ozsahin, and S. Askar, "Computation of stagnation coating flow of electro-conductive ternary williamson hybrid GO-AU-$Co_3O_4$/EO nanofluid with a cattaneo–christov heat flux model and magnetic induction," Sci. Rep. **13**, 10972 (2023).

[32]M. E. Piyasena, G. P. Lopez, and D. N. Petsev, "An electrokinetic cell model for analysis and optimization of electroosmotic microfluidic pumps," Sens. Actuators B Chem. **113**, 461–467 (2006).

[33]J. Wu, W. Wen, and P. Sheng, "Smart electroresponsive droplets in microfluidics," Soft Matter **8**, 11589–11599 (2012).

[34]N. Vennela, S. Mondal, S. De, and S. Bhattacharjee, "Sherwood number in flow through parallel porous plates (microchannel) due to pressure and electroosmotic flow," AIChE J. **58**, 1693–1703 (2012).

[35]M. G. Reddy, D. Tripathi, O. A. Bég, and A. K. Tiwari, "Numerical modelling of elec-tromagnetohydrodynamic (emhd) radiative transport of hybrid $Ti_6Al_4V-AA7075/H_2O$ nanofluids from a riga plate sensor surface," in *Nanomaterials and Nanoliquids: Applica- tions in Energy and Environment*, edited by D. Tripathi, R. K. Sharma, H. F. Oztop, and R. Natarajan (Springer Nature, Singapore, 2023) pp. 225–248.

[36]G. Mao, D. Schiller, D. Danninger, B. Hailegnaw, F. Hartmann, T. Stockinger, M. Drack, N. Arnold, and M. Kaltenbrunner, "Ultrafast small-scale soft electromagnetic robots," Nat. Commun. **13**, 4456 (2022).

[37]O. A. Bég, M. Hameed, and T. A. Bég, "Chebyshev spectral collocation simulation of nonlinear boundary value problems in electrohydrodynamics," Int. J. Comput. Methods Eng. Sci. Mech. **14**, 104–115 (2013).

[38]Y. Yang, D. Li, Y. Sun, M. Wu, J. Su, Y. Li, X. Yu, L. Li, and J. Yu, "Muscle-inspired soft robots

based on bilateral dielectric elastomer actuators," Microsyst. Nanoeng. **9**, 124 (2023).

[39]Y. Ren, W. Cui, and S. Li, "Electrohydrodynamic instability of premixed flames under manipulations of dc electric fields," Phys. Rev. E **97**, 013103 (2018).

[40]D. Tripathi, A. Sharma, O. A. Bég, and A. Tiwari, "Electrothermal transport in biolog- ical systems: an analytical approach for electrokinetically modulated peristaltic flow," J. Therm. Sci. Eng. Appl. **9**, 041010 (2017).

[41]G. D. Harvel, B. Komeili, C. Y. Ching, and J. Chang, "Electrohydrodynamically enhanced capillary evaporator," IEEE Trans. Dielectr. Electr. Insul. **16**, 456–462 (2009).

[42]V. K. Narla, D. Tripathi, D. S. Bhandari, and O. A. Bég, "Electrokinetic insect-bioinspired embrane pumping in a high aspect ratio bio-microfluidic system," Microfluid. Nanofluid. **26**, 85 (2022).

[43]W. D. Ristenpart, I. A. Aksay, and D. A. Saville, "Electrically driven flow near a colloidal particle close to an electrode with a faradaic current," Langmuir **23**, 4071–4080 (2007).

[44]P. Rana, N. Shukla, O. A. Bég, A. Kadir, and B. Singh, "Unsteady electromagnetic radiative nanofluid stagnation-point flow from a stretching sheet with chemically reactive nanoparticles, Stefan blowing effect and entropy generation," Proc. Inst. Mech. Eng. N J. Nanomater. Nanoeng. Nanosyst. **232**, 69–82 (2018).

[45]S. K. Griffiths and R. H. Nilson, "Hydrodynamic dispersion of a neutral nonreacting solute in electroosmotic flow," Anal. Chem. **71**, 5522–5529 (1999).

[46]A. K. Roy, S. Debnath, and O. A. Bég, "Transient solute dispersion in electro-osmotic viscoplastic flow in a microchannel," ZAMM **103**, e202200260 (2023).

[47]M. Sadeghi, M. H. Saidi, A. Moosavi, and A. Sadeghi, "Unsteady solute dispersion by electrokinetic flow in a polyelectrolyte layer-grafted rectangular microchannel with wall absorption," J. Fluid Mech. **887** (2020), 10.1017/jfm.2019.1083.

[48]V. Hoshyargar, A. Khorami, S. N. Ashrafizadeh, and A. Sadeghi, "Solute dispersion by electroosmotic flow through soft microchannels," Sens. Actuators B Chem. **255**, 3585–3600 (2018).

[49]D. Murugan, A. K. Roy, R. Ponalagusamy, and O. A. Bég, "Tracer dispersion due to pulsatile Casson fluid flow in a circular tube with chemical reaction modulated by externally applied electromagnetic

fields," Int. J. Appl. Comput. Math. **8**, 221 (2022).

[50]S. Paul and C.-O. Ng, "Dispersion in electroosmotic flow generated by oscillatory electric field interacting with oscillatory wall potentials," Microfluid. Nanofluid. **12**, 237–256 (2012).

[51]S. Paul and C.-O. Ng, "On the time development of dispersion in electroosmotic flow through a rectangular channel," Acta Mech. Sin. **28**, 631–643 (2012).

[52]J. Song, C.-O. Ng, and W.-K. A. Law, "Dispersion in oscillatory electro-osmotic flow through a parallel-plate channel with kinetic sorptive exchange at walls," J. Hydrodyn. **26**, 363–373 (2014).

[53]K. K. Mondal, S. Dhar, and B. S. Mazumder, "On dispersion of solute in steady flow through a channel with absorption boundary: an application to sewage dispersion," Theor. Comput. Fluid Dyn. **34**, 643–658 (2020).

[54]N. Poddar, S. Dhar, B. S. Mazumder, R. R. Kairi, and K. K. Mondal, "Effects of bulk degradation and boundary absorption on dispersion of contaminant in wetland flow," Int. J. Heat Mass Transfer **179**, 121669 (2021).

[55]H. Wang, Y. Ai, J. Zhang, Z. Zhu, W. Wang, Y. Jin, and W. Huai, "Analysis of contaminant dispersion in open channel with two streambank-absorption boundaries," Environ. Sci. Pollut. Res. **30**, 654–665 (2023).

[56]D. Das, K. K. Mondal, N. Poddar, and P. Wang, "Transient dispersion of a reactive solute in an oscillatory couette flow through an anisotropic porous medium," Phys. Fluids **36**, 023610 (2024).

[57]D. A. Saville, "Electrohydrodynamics: the Taylor-Melcher leaky dielectric model," Annu. Rev. Fluid Mech. **29**, 27–64 (1997).

[58]W. N. Gill, "A note on the solution of transient dispersion problems," Proc. R. Soc. A **298**, 335–339 (1967).

[59]R. Sankarasubramanian and W. N. Gill, "Unsteady convective diffusion with interphase mass transfer," Proc. R. Soc. A **333**, 115–132 (1973).

[60]W. Q. Jiang and G. Q. Chen, "Solution of Gill's generalized dispersion model: solute transport in Poiseuille flow with wall absorption," Int. J. Heat Mass Transf. **127**, 34–43 (2018).

[61]S. Debnath, W. Jiang, M. Guan, and G. Chen, "Effect of ring-source release on dispersion process in poiseuille flow with wall absorption," Phys. Fluids **34**, 027106 (2022).

[62]J. S. Yu and W. S. Chang, "Dispersion of solute in wall-bounded parallel shear flows," J. Eng. Math. **25**, 31–62 (1991).

[63]T. Y. Lin and E. S. G. Shaqfeh, "Taylor dispersion in the presence of cross flow and interfacial mass transfer," Phys. Rev. Fluids **4**, 034501 (2019).

[64]R. Erban and S. J. Chapman, *Stochastic Modelling of Reaction–Diffusion Processes* (Cam- bridge Univ. Press, Cambridge, 2020).

[65]W. Jiang, L. Zeng, X. Fu, and Z. Wu, "Analytical solutions for reactive shear dispersion with boundary adsorption and desorption," J. Fluid Mech. **947**, A37 (2022).

[66]B. Wang, W. Jiang, G. Chen, and L. Tao, "Transient dispersion in a channel with crossflow and wall adsorption," Phys. Rev. Fluids **7**, 074501 (2022).

[67]R. Erban and S. J. Chapman, "Reactive boundary conditions for stochastic simulations of reaction–diffusion processes," Phys. Biol. **4**, 16–28 (2007).

[68]X. Fu, R. Gao, and Z. Wu, "Additional longitudinal displacement for contaminant dispersion in wetland flow," J. Hydrol. **532**, 37–45 (2016).

[69]J. Guo, X. Wu, W. Jiang, and G. Chen, "Contaminant transport from point source on water surface in open channel flow with bed absorption," J. Hydrol. **561**, 295–303 (2018).

[70]P. Wang, L. Zeng, and W. Huai, "Transient dispersion of an initial point pollutant concentration in wetland flows," Environ. Sci. Pollut. Res. **25**, 34414–34425 (2018).

[71]Y.-D. Ai, H.-C. Dai, Y.-W. Zhai, B. Chen, and W.-X. Huai, "The effect of solute re- lease position on transient solute dispersion in floating wetlands: An analytical study," J. Cleaner Prod. **369**, 133370 (2022).

[72]A. Stuart and J. K. Ord, *The advanced theory of statistics*, 6th ed., Vol. 1: Distribution theory (Wiley, Hoboken, NJ, USA, 2010).

[73]P. C. Chatwin, "The cumulants of the distribution of concentration of a solute dispersing in solvent

flowing through a tube," J. Fluid Mech. **51**, 63–67 (1972).

[74]W. Jiang and G. Chen, "Solute transport in two-zone packed tube flow: Long-time asymptotic expansion," Phys. Fluids **31**, 043303 (2019).

[75]I. Frankel and H. Brenner, "On the foundations of generalized Taylor dispersion theory," J. Fluid Mech. **204**, 97–119 (1989).

[76]G. Li, W. Jiang, P. Wang, J. Guo, Z. Li, and G. Q. Chen, "Concentration moments based analytical study on Taylor dispersion: open channel flow driven by gravity and wind," J. Hydrol. **562**, 244–253 (2018).

[77]N. G. Barton, "On the method of moments for solute dispersion," J. Fluid Mech. **126**, 205–218 (1983).

[78]A. D. Polyanin, *Handbook of Linear Partial Differential Equations for Engineers and Scientists* (Chapman and Hall/CRC, New York, 2001).

[79]P. Wang and G. Q. Chen, "Basic characteristics of Taylor dispersion in a laminar tube flow with wall absorption: exchange rate, advection velocity, dispersivity, skewness and kurtosis in their full time dependence," Int. J. Heat Mass Transf. **109**, 844–852 (2017).

[80]Y. Yang, W. Q. Jiang, Y. H. Wu, P. Wang, Z. Wu, B. Zhang, and L. Zeng, "Migration of buoyancy-controlled active particles in a laminar open-channel flow," Adv. Water Resour. **156**, 104023 (2021).